



RESEARCH ARTICLE

10.1002/2015PA002882

Key Points:

- Abyssal northwest Pacific records show cyclic glacial magnetite dissolution zones
- Evidence for glacial carbon trapping in sediment followed by deglacial CO₂ release
- Changing LCDW/AABW partitioning from Atlantic to Pacific after mid-Pleistocene transition

Correspondence to:

T. von Dobeneck,
dobeneck@uni-bremen.de

Citation:

Korff, L., T. von Dobeneck, T. Frederichs, S. Kasten, G. Kuhn, R. Gersonde, and B. Diekmann (2016), Cyclic magnetite dissolution in Pleistocene sediments of the abyssal northwest Pacific Ocean: Evidence for glacial oxygen depletion and carbon trapping, *Paleoceanography*, 31, 600–624, doi:10.1002/2015PA002882.

Received 21 SEP 2015

Accepted 29 APR 2016

Accepted article online 7 MAY 2016

Published online 24 MAY 2016

Cyclic magnetite dissolution in Pleistocene sediments of the abyssal northwest Pacific Ocean: Evidence for glacial oxygen depletion and carbon trapping

Lucia Korff¹, Tilo von Dobeneck¹, Thomas Frederichs¹, Sabine Kasten^{1,2}, Gerhard Kuhn^{1,2}, Rainer Gersonde^{1,2}, and Bernhard Diekmann³

¹MARUM—Center for Marine Environmental Sciences and Faculty of Geosciences, University of Bremen, Bremen, Germany,

²Alfred Wegener Institute, Helmholtz Centre for Polar and Marine Research, Bremerhaven, Germany, ³Alfred Wegener Institute, Helmholtz Centre for Polar and Marine Research, Potsdam, Germany

Abstract The carbonate-free abyss of the North Pacific defies most paleoceanographic proxy methods and hence remains a “blank spot” in ocean and climate history. Paleomagnetic and rock magnetic, geochemical, and sedimentological methods were combined to date and analyze seven middle to late Pleistocene northwest Pacific sediment cores from water depths of 5100 to 5700 m. Besides largely coherent tephra layers, the most striking features of these records are nearly magnetite-free zones corresponding to glacial marine isotope stages (MISs) 22, 12, 10, 8, 6, and 2. Magnetite depletion is correlated with organic carbon and quartz content and anticorrelated with biogenic barite and opal content. Within interglacial sections and mid-Pleistocene transition glacial stages MIS 20, 18, 16, and 14, magnetite fractions of detrital, volcanic, and bacterial origin are all well preserved. Such alternating successions of magnetic iron mineral preservation and depletion are known from sapropel-marl cycles, which accumulated under periodically changing bottom water oxygen and redox conditions. In the open central northwest Pacific Ocean, the only conceivable mechanism to cause such abrupt change is a modified glacial bottom water circulation. During all major glaciations since MIS 12, oxygen-depleted Antarctic Bottom Water (AABW)-sourced bottom water seems to have crept into the abyssal northwest Pacific below ~5000 m depth, thereby changing redox conditions in the sediment, trapping and preserving dissolved and particulate organic matter and, in consequence, reducing and dissolving both, biogenic and detrital magnetite. At deglaciation, a downward progressing oxidation front apparently remineralized and released these sedimentary carbon reservoirs without replenishing the magnetite losses.

1. Introduction

The abyssal North Pacific Ocean's large volume, depth, and terminal position on the deep oceanic conveyor make it a candidate site for deep carbon trapping as postulated by climate theory to explain the massive glacial drawdown of atmospheric CO₂ [e.g., *Toggweiler*, 1999; *Sigman and Boyle*, 2000; *Galbraith et al.*, 2007; *Adkins*, 2013]. Cyclic stagnation and oxygen depletion of abyssal Pacific bottom water masses have been suggested by several authors [*Matsumoto et al.*, 2002; *Jaccard et al.*, 2009, 2010, 2016] and could have enabled an enhanced storage of dissolved inorganic carbon (DIC) in the deep ocean [*Bradt Miller et al.*, 2010]. Newer results show that dissolved organic matter (DOM) has longer residence times in the ocean and may have acted as another deep carbon pool controlling past ocean conditions [*Lechtenfeld et al.*, 2014; *Hansell and Carlson*, 2013]. Here we seek rock magnetic and sedimentological evidence for temporary glacial redox changes supporting particulate organic matter (POM) storage in surficial sediments of the abyssal northwest Pacific Ocean and develop ideas about potential budgets, residence times, and climate relevance. While abyssal POM deposits were certainly much smaller glacial carbon reservoirs compared to deep ocean DIC and DOM pools [*Sigman and Boyle*, 2000], their potential long-term sequestration, deglacial release, and geochemical reactivity appear to be relevant.

The major abyssal basins of the North Pacific have depths of 5500–6500 m, far below the modern and glacial calcite compensation depths (CCD) presently located at ~4500 m [*Berger et al.*, 1976]. Carbonate-based proxy reconstructions of the deep North Pacific circulation [e.g., *Keigwin*, 1998; *Ohkushi et al.*, 2003; *Herguera et al.*, 2010] are therefore restricted to isolated seamounts and submarine plateaus towering more than 2000 m above the abyssal basins. To our knowledge, carbonate-free basin sediments have not yet been purposely studied in the context of deep water reconstruction.

Paleomagnetic, rock, and environmental magnetic methods are generally well applicable to unfossiliferous abyssal muds and clays. Previous magnetic studies on these materials were mainly concerned with reversal magnetostratigraphy [e.g., *Ninkovich et al.*, 1966; *Kent and Lowrie*, 1974; *Bleil*, 1985; *Yamazaki and Kanamatsu*, 2007] and terrigenous input changes [e.g., *Doh et al.*, 1988; *Yamazaki and Ioka*, 1997; *Yamazaki*, 1999]. In other temporarily oxygen-depleted basins like the Mediterranean Sea, the redox sensitivity of magnetic iron oxide minerals has already been used to reconstruct bottom water ventilation and sapropel formation from magnetite depletion records [e.g., *Larrasoña et al.*, 2003]. Partial magnetite dissolution in Equatorial Atlantic pelagic sequences was interpreted by *Funk et al.* [2004a, 2004b] in terms of higher POM burial during glacial periods. We apply their enviromagnetic proxy methods to the sub-CCD piston core SO202-39-3 from the abyssal northwest Pacific (5102 m). This core is part of an ocean-wide North Pacific west-east core transect at 38–40°N collected in 2009 by the RV SONNE INOPEX expedition (Innovative North Pacific Experiment). We correlate and expand our findings to six adjacent cores from water depths between 5200 and 5700 m.

The process chain of carbon production, export, and sequestration in North Pacific Ocean basins during the Pleistocene involves several potential drivers: changing nutrient supply and bioproductivity [*Yamane*, 2003; *Shigemitsu et al.*, 2007; *Jaccard et al.*, 2009], enhanced scavenging of surface ocean organic carbon by intensified glacial Asian dust input [*Maeda et al.*, 2002], lower temperature and reduced exchange of the North Pacific Deep and Bottom Waters enabling higher CO₂ intake [*Jaccard et al.*, 2005; *Matsumoto et al.*, 2002], and better POM preservation at and below the seafloor due to lower sedimentary oxygenation levels [*Sigman and Boyle*, 2000] and remineralization rates [*Hartnett et al.*, 1998]. We reconstruct time series of some of these environmental factors over the past 940 kyr using high-resolution sedimentary records associated with organic carbon export and preservation (Ba/Ti, opal, and total organic carbon (TOC)), eolian input (quartz, mica, and HIRM), volcanic input (κ and isothermal remanent magnetization (IRM)), and reductive magnetite dissolution (anhysteretic remanent magnetization (ARM), ARM/IRM, $S_{0.3T}$, and Fe/ κ). These results merge into a conceptual geochemical process model and simple budget estimate of temporary glacial POM storage in the abyssal sediments of the northwest and the entire deep Pacific Ocean.

2. Hydrography and Sedimentology of the Northwest Pacific

2.1. Hydrography

The northwest Pacific is the world's deepest ocean basin dipping from ~5000 m depth to more than 6000 m depth (Figure 1). The investigated core transect (SO202-38 to SO202-45; water depths 5102–5670 m) spans the central basin at 40–38°N latitude from 169° to 149°E longitude. This is just south of the confluence zone of the two northwest Pacific coastal currents, the cold subarctic Oyashio Current and the warm subtropical Kuroshio Current. Their deflection points define the North Pacific subarctic front dividing subarctic Pacific Water from Western North Pacific Central Water [*Tomczak and Godfrey*, 2003; *Maeda et al.*, 2002]. This front also delimits the glacial southward iceberg drift from the western Bering Sea and the east coast of Kamchatka Peninsula to the northwest Pacific throughout the entire Pleistocene [*St. John and Krissek*, 1999]. Ice-rafted debris should therefore be very rare in our cores, particularly at the easterly sites.

Nutrient-poor, well-ventilated North Pacific Intermediate Water (NPIW) sourced from the Okhotsk Sea outflow and western subpolar gyre [*You et al.*, 2000; *You*, 2003] occupies depths of ~300–2000 m in the northwest Pacific. Below is the North Pacific Deep Water (NPDW) sourced from Lower Circumpolar Deep Water (LCDW) supplied by the Southwest Pacific Deep Western Boundary Current (DWBC). The DWBC reaches the North Pacific through the Samoan Passage, the ~5000 m deep “choke point” of LCDW flow to the abyssal North Pacific [*Reid and Lonsdale*, 1974]. At the submarine “Mid-Pacific Mountains” confining the northwest Pacific Basin in the south, the bottom current bifurcates into a western (4.1 ± 1.2 sverdrup (Sv)) and a larger and deeper eastern (9.8 ± 1.8 Sv) branch [*Owens and Warren*, 2001; *Yanagimoto et al.*, 2010]. The coldest and most saline LCDW water passes through the Wake Island Passage (~5180 m) into the northwest Pacific Basin [*Uchida et al.*, 2007] and forms the modern bottom water mass [*Fukasawa et al.*, 2004]. It flows counterclockwise through the subbasin formed by the Emperor Seamount Chain and the Shatsky Rise [*Yanagimoto and Kawabe*, 2007], a Mesozoic igneous plateau [*Nakanishi et al.*, 1989] rising up to 1962 m below sea level. The western, shallower branch of the deep water current follows the Mariana Arc and meets the deeper eastern branch off Japan, from where it follows the western Kuril-Kamchatka Arcs to finally overflow to the

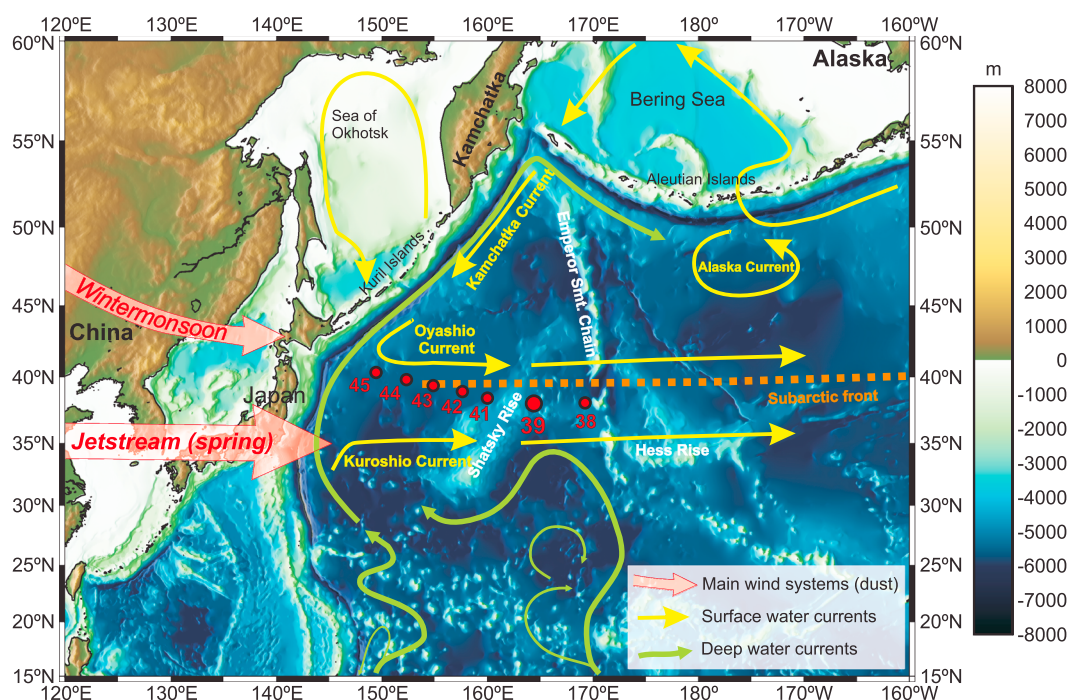


Figure 1. Bathymetric map of the NW Pacific Ocean and its marginal seas, showing piston core locations (red dots) of RV SONNE cruise SO202 (INOPEX), major dust trajectories (after Nilson and Lehmkuhl [2001], in light red) and main ocean currents. Surface currents [Maslin et al., 1998] are marked with yellow arrows and deep water currents (after Yanagimoto and Kawabe [2007] and Owens and Warren [2001]) with green arrows.

Northeast Pacific basin between the Aleutian Arc and the Detroit Seamount. Yanagimoto et al. [2010] determined bottom currents of ~1–5 cm/s southwest of the Shatsky Rise implying a relatively slow but continuous bottom water exchange. The northward reach of Antarctic Bottom Water (AABW) from the abyssal South and Central Pacific basins is now limited to ~20°N.

Under modern conditions, the water column below 2000 m depth is well oxygenated (3–4 mL/L), while lower oxygen levels (1–2 mL/L) are found in the O₂ minimum zone at 1000–2000 m depth [Kawabe et al., 2009]. Many authors argued that this situation should have been reversed during glacial periods [Duplessy et al., 1988; Keigwin, 1998; Matsumoto et al., 2002; Okazaki et al., 2012; Sigman and Boyle, 2000; Sigman et al., 2010]. Under conditions of reduced Antarctic overturning and shallower North Atlantic ventilation, the fresher and lighter Glacial North Atlantic Intermediate Water (GNAIW) should have surrounded Antarctica at midwater depths to ventilate the glacial deep water mass of the North Pacific. Below a northern sourced, nutrient- and oxygen-poor NPIW cover extending down to 2000 m, this southern sourced nutrient-rich and well oxygenated glacial NPDW layer is thought to have circulated clockwise over the entire North Pacific from 2000 to 4000 m depth, thereby stabilizing the CCD depth and invoking higher benthic δ¹³C values [Duplessy et al., 1988; Herguera et al., 1992; Keigwin, 1998; Matsumoto et al., 2002]. But underneath the NPDW, ultracold and ultrasaline Antarctic Bottom Water (AABW) could have crept into the glacial North Pacific abyss [Ronge et al., 2015], creating a stagnant, oxygen-depleted abyssal water mass below ~5000 m, a perfect trap for settling organic matter [Sigman and Boyle, 2000].

Several studies support the assumption that the primary production in the subarctic northwest Pacific was lower during glacial periods [Galbraith et al., 2008; Gebhardt et al., 2008; Jaccard et al., 2005, 2009; Shigemitsu et al., 2007] due to reduced nutrient supplies from subsurface waters [Jaccard et al., 2010]. Other authors speak of increased primary production during glacial periods [Yamane, 2003] in view of enhanced TOC, biogenic opal, and CaCO₃ mass accumulation rates. Both conflicting notions can be reconciled by assuming a more efficient glacial carbon export to the deep ocean due to higher dust fluxes and intensified scavenging; better preservation conditions for particulate organic carbon in abyssal surface sediments would result from lower oxygenation and lower temperatures [Matsumoto, 2007; Jaccard et al., 2010].

2.2. Sedimentology

Below the modern CCD situated at ~4100–4400 m in the central northwest Pacific [Berger *et al.*, 1976], 80–90% of the abyssal sediments are of terrigenous origin [Blank *et al.*, 1985]. The complementary 10–20% are biogenic and composed of siliceous microfossils [Shigemitsu *et al.*, 2007], while marine carbonate is nearly absent. The dominant terrigenous component is eolian dust, uplifted by strong wind gusts from the large arid regions in China and Mongolia, the Taklimakan desert in northwest China, and the deserts of Inner Mongolia [e.g., Serno *et al.*, 2014] and carried seaward by upper level westerly winds (jetstream) and lower level northwesterly winds (Eastern Asian winter monsoon) [Nilson and Lehmkuhl, 2001]. East Asian shelves falling dry during glacial sea level lowstands have been considered as additional, more proximal dust sources of the northwest Pacific [Nichol and Nichol, 2013]. Loess accumulation in China and dust deposition in the Pacific show equivalent changes in composition and flux [Hovan *et al.*, 1989, 1991; Balsam *et al.*, 2005; Maher *et al.*, 2010]. Dust accumulation rates in the central northwest Pacific were generally 2–3 times higher during the Last Glacial Maximum (LGM) as compared to Holocene levels [Rea, 1994; Kohfeld and Harrison, 2001; Balsam *et al.*, 2005; Shigemitsu *et al.*, 2007].

Intercalated fine volcanic ash and pumice layers (mostly 1–2 cm, some 10 cm) are frequent in sediments from the Shatsky Rise area and have been backtracked to recently active volcanoes on Hokkaido and the Kuril Islands [Natland, 1993]. According to Natland's estimates, the number of observable tephra layers per Myrs should decline from ~30 in the west to ~5 in the east of our core transect. A well-established chronostratigraphic marker in the study area is tephra layer Aso-4 (~87 ka) in marine isotope stage (MIS) 5b [Aoki, 2008].

3. Materials and Methods

3.1. Materials

From 7 July to 29 August 2009, the international paleoceanographic research cruise SO202-INOPEX (Innovative North Pacific Experiment) by the German RV SONNE collected two ocean-spanning EW sediment core transects of the North Pacific and Bering Sea [Gersonde, 2012], recovering a total of 50 piston and gravity cores from 45 sites. Out of seven here considered abyssal northwest Pacific piston cores (SO202-38, -39, -41, -42, -43, -44, and -45; Figure 1) with mostly coherent shipboard susceptibility logs, the 20.23 m long SO202-39-3 retrieved from 5102 m water depth east of northern Shatsky Rise (38°00.70'N, 164°26.78'E) was rated as the stratigraphically most promising record of the entire core transect and selected for detailed paleomagnetic and rock magnetic, geochemical, and sedimentological investigations. Its relatively distal location from active volcanism and the Asian continent should result in lesser disturbance by tephra layers and coverage of a full middle to late Pleistocene sequence and the Brunhes/Matuyama geomagnetic field reversal.

The sediment lithology of SO202-39-3 is described as lightly to moderately mottled diatomaceous mud or mud-bearing diatom ooze with traces of radiolarians. Sediment porosity shows very constant values of ~84% throughout the core [Gersonde, 2012]. Sediment colors vary between yellowish to brownish and greyish to greenish hues (Figure 2). Three distinct ash layers at core depths of 1.76–1.785 m, 13.82–13.87 m, and 16.30–16.37 m could be identified by smear slide analyses. Glass shards indicating subordinate volcanic contributions were frequently found throughout the core. The uppermost ~35 cm section of the core appears to have been slightly disturbed by the coring process. For paleomagnetic and rock magnetic investigations, a total of 406 oriented standard plastic sample cubes of 6.2 cm³ volume was taken at 5 cm depth increments throughout the core.

3.2. Paleomagnetic and Rock Magnetic Methods

Magnetic volume susceptibility κ is the ratio of sample magnetization change per applied external magnetic field change. It is unitless in the SI unit system, which we signalize by the letters "SI" after the ratio value. κ was measured on all full cores at increments of 2 cm using a shipboard GEOTEK Multi-Sensor Core Logger (MSCL) equipped with a Bartington M.S.2 susceptibility meter and a 140 mm loop sensor. Sharp lithology changes (e.g., ash layers and dropstones) are smoothed in these susceptibility data due to the coil size related averaging over a core interval of about 8 cm (half width of sensor characteristic). Magnetic volume susceptibility κ was also measured on cube samples using a Geofyzika KappaBridge KLY-2 susceptometer for better comparability with sample-based remanence measurements. Magnetic susceptibility is an integral measure of field-induced magnetization by diamagnetic, paramagnetic, and ferrimagnetic sedimentary minerals.

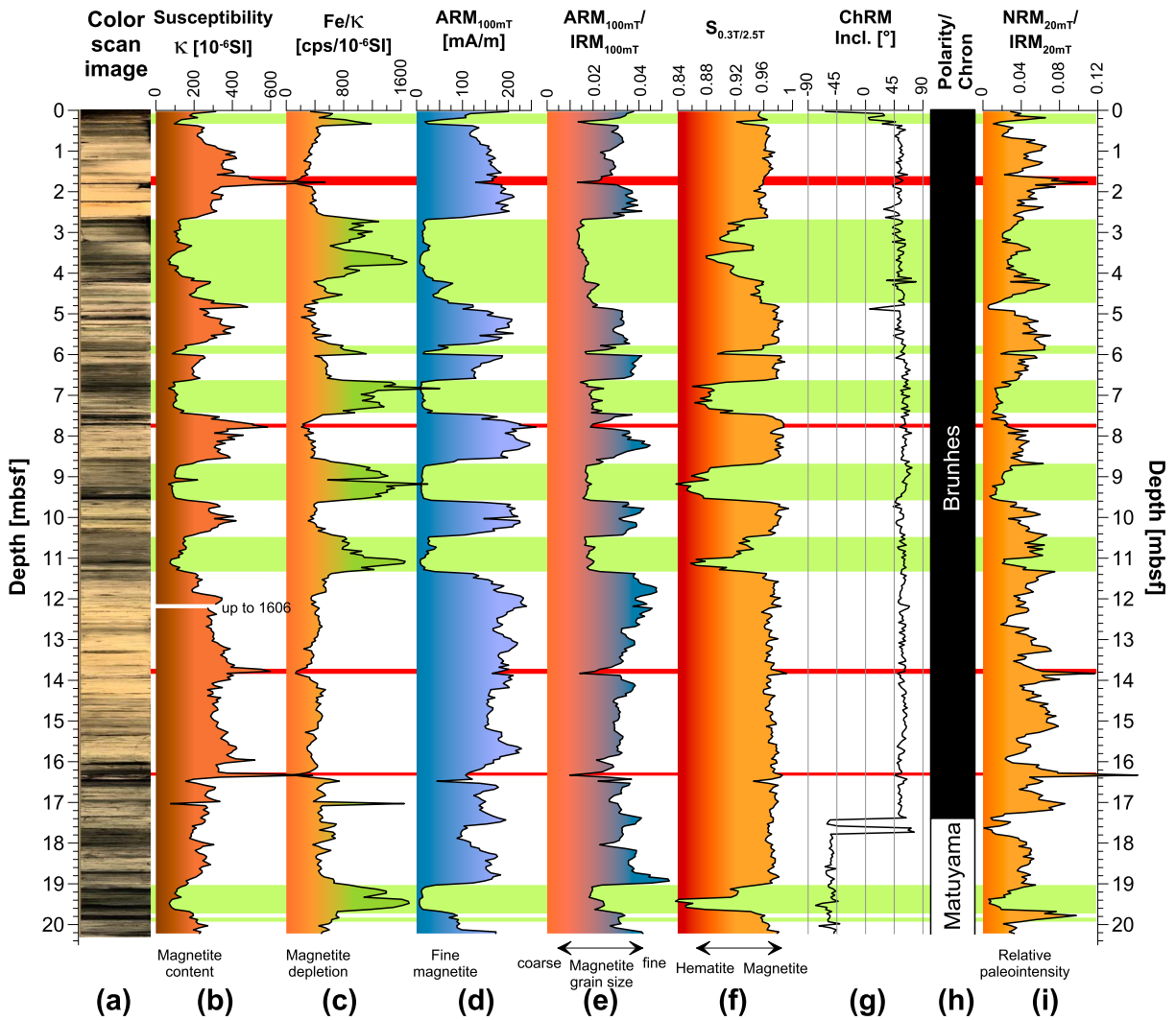
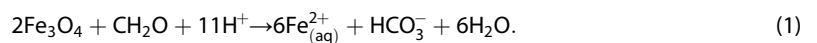


Figure 2. (a) Sediment color, (b–f) selected rock magnetic, and (g, i) paleomagnetic parameters of piston core SO202-39-3 versus depth. (h) The Brunhes/Matuyama polarity reversal. Green shaded bars mark zones of magnetite depletion. They correspond to darker sediment colors (Figure 2a), high Fe/κ values (Figure 2c), and lower values in parameters b, d, e, and f, indicating a loss of fine magnetite. Red bars highlight tephra layers, which can be identified visually [Gersonde, 2012] and from prominent values in parameters b and e.

Above a baseline value set by the balance of paramagnetism and diamagnetism, variations in κ delineate primarily concentration changes of ferrimagnetic iron oxide minerals ((Ti-)magnetite, (Ti-)maghemite, (Ti-)hematite) and iron sulfide minerals (greigite and pyrrhotite), which only form in the presence of free HS⁻ [e.g., Fu et al., 2008].

Suboxic sedimentary environments typically experience a gradual reduction of ferric (Fe(III)-bearing) minerals such as magnetite, hematite, goethite, lepidocrocite, ferrihydrite, and Fe-rich silicates, whose Fe³⁺ cations serve as electron acceptors to remineralize organic carbon in absence of oxygen and nitrate:



The proxy ratio Fe/κ [Funk et al., 2004a] compares magnetite content with total iron content, which at first reflects the magnetic petrology of the terrigenous fraction. At oceanic sites with distal continental sources, this starting value is typically a very stable number through time, in particular, if corrected for diluting diamagnetic marine components (CaCO₃, H₂O, and SiO₂). In particular submicron magnetite particles with their high specific surface are rapidly dissolved by iron reduction during suboxic carbon remineralization. The released Fe²⁺ ions reprecipitate as very weakly magnetic oxyhydroxides or sulfides [Karlin, 1990;

Tarduno, 1994; Hounslow and Maher, 1999; Roberts et al., 1999]. Dissolution of primary magnetite is irreversible and increasingly lowers κ relative to pristine conditions. The resulting increase of Fe/ κ relative to a baseline value quantifies the transformation grade of high- κ magnetite into low- κ paramagnetic Fe minerals. In some cases upward migrating Fe²⁺ ions are precipitated at the Fe³⁺/Fe²⁺ redox boundary as secondary magnetite by microbial biomineralization creating an inverse Fe/ κ peak just above the diagenetic layer [Tarduno, 1994; Tarduno and Wilkison, 1996; Larrasoña et al., 2003; Funk et al., 2004a].

A range of natural and artificial magnetic remanences (unit A/m) was measured on all cube samples using the 2G Cryogenic Rock Magnetometer of the Marine Geophysics Section at University of Bremen. Fundamentals and aims of environmental magnetic techniques and parameters were described, e.g., by Thompson and Oldfield [1986], Stoner et al. [1996], Maher and Thompson [1999], and Frederichs et al. [1999]. We chose to combine two paleomagnetic methods, reversal magnetostratigraphy and relative paleointensity (RPI) correlation, to establish a climate-independent magnetostratigraphic age model for our core. These methods have been successfully used for numerous carbonate-free abyssal sediment cores from the North Pacific [e.g., Ninkovich et al., 1966; Bleil, 1985; Roberts et al., 1997; Yamazaki and Kanamatsu, 2007; Yamamoto et al., 2007].

A detailed alternating field demagnetization of the natural remanent magnetization (NRM) was performed in 16 steps up to 100 mT. The characteristic remanent magnetization (ChRM) was calculated using the principle component analysis method of Kirschvink [1980]. Stable directions were generally reached after 5 mT alternating field demagnetization. We only show ChRM inclinations here, which show more consistent patterns than declinations. For RPI, NRM was normalized by isothermal remanent magnetization (IRM), as anhysteretic remanent magnetization (ARM) is more biased by magnetite dissolution. ARM is also known to be sensitive for magnetic interaction effects and can overcompensate changes in carrier concentration [Yamazaki and Kanamatsu, 2007]. Susceptibility is not practical as NRM normalizer here because of the high paramagnetic background. RPI records were calculated as NRM/IRM ratios after demagnetizing both remanences in peak alternating fields of 20 mT to remove a possible viscous overprint.

ARM was imparted in a peak alternating field of 100 mT with a superimposed bias field of 0.04 mT. ARM is used as a grain size selective parameter assessing the content of fine-grained, single domain (30 nm < d < 100 nm), and pseudo-single domain (100 nm < d < 1 μ m) magnetite particles [King et al., 1982; Maher, 1988; Stoner et al., 1996]. These fine magnetite particles are particularly susceptible to dissolution under reducing conditions [Karlin et al., 1987; Bloemendal et al., 1992; Larrasoña et al., 2003; Funk et al., 2004a, 2004b]. IRM was automatically imparted in 16 field steps up to 700 mT with an in-line pulse magnetizer. Higher fields up to 2500 mT were manually applied with an external pulse magnetizer. The peak IRM is referred to as SIRM (saturation IRM). IRM quantifies the concentrations of ferrimagnetic and (spin canting or defect, i.e., imperfect) antiferromagnetic minerals depending of their coercivity (magnetic stability).

ARM/IRM and $\kappa_{\text{ARM}}/\kappa$ are commonly used and largely similar “magnetogranulometric” proxy ratios for the magnetite domain state, i.e., for the median crystal size of magnetite [Maher, 1988]. Smaller values indicate larger median grain size. The latter ratio can be biased by diamagnetism and paramagnetism in magnetite-impooverished environments. The approach is not applicable for ultrasmall (<30 nm) superparamagnetic particles and for very coarse sediments (>100 μ m). “Hard” IRM (HIRM) was calculated by subtracting IRM_{0.3T} from SIRM. HIRM primarily varies with the concentration of the (imperfectly) antiferromagnetic minerals hematite and goethite. The parameter $S_{-0.3T}$ (here $S_{0.3T} = \text{IRM}_{0.3T}/\text{SIRM}$) is a nonlinear ratio number of ferrimagnetic vs. antiferromagnetic mineral content [Bloemendal et al., 1992]. Values close to 1 indicate a magnetic (not volumetric!) dominance of low-coercivity ferrimagnetic minerals, while increasingly smaller values indicate stronger influence of high-coercivity antiferromagnetic minerals.

3.3. Sedimentological and Geochemical Methods

For analyzing sedimentary organic carbon, biogenic carbonate and opal content, about 10 cm³ of sediment, were sampled every 10 cm. Total organic carbon (TOC) content was measured with an Eltra CS2000 elemental analyzer after carbonate removal. Biogenic opal content was determined from the temporal leaching function after Müller and Schneider [1993] assuming a reasonable 10 wt % H₂O content.

The mineralogical composition of sediment core SO202-39-3 was determined on 215 samples at 10 cm steps. Bulk powder samples were analyzed by X-ray diffractometry (XRD) using a Philips PW1820 goniometer at AWI Bremerhaven (40 kV, 40 mA, from 3 to 100°, step rate 0.05°, Co α radiation). XRD data were analyzed using

MacDiff 4.0.7 (freeware by Rainer Petschick, University Frankfurt). Peak area intensities of the minerals quartz (4.26 Å) and mica (10 Å) are plotted as indicators of terrigenous components in the bulk sediment.

The 10 µm resolution red-green-blue color scans of all core segments were taken with a *GEOTEK GEOSCAN II* camera soon after splitting to minimize color changes upon exposure to air. Major element abundances (Fe, Ba, Ti, and Al) were determined by XRF core scanning (XRF-CS) using the *Avaatech XRF* core scanner at AWI Bremerhaven at 1 cm resolution. Here they are given as uncalibrated peak area counts per second (cps). Element ratios (e.g., Ba/Ti) are presented to compensate for matrix effects of the wet sediment [Tjallingii et al., 2007].

Biogenic barite in marine sediments is commonly used as a proxy for paleoproductivity [e.g., *Dehairs et al.*, 1980; *Dymond et al.*, 1992; *Gingele and Dahmke*, 1994; *Pfeifer et al.*, 2001]. Biogenic barite crystals are thought to form in the oxic water column during the decay of descending organic matter within Ba-supersaturated microenvironments [e.g., *Dehairs et al.*, 1980; *Bishop*, 1988; *Ganeshram et al.*, 2003]. Under oxic to suboxic conditions, the preservation potential for barite (~30% of total flux) is far better than for organic carbon (<1%) and biogenic silica (<5%) [Paytan and Kastner, 1996]. Only in sedimentary environments with depleted pore water sulfate is barite dissolved and barium mobilized, which then disables its use as a paleoproductivity proxy [e.g., *Dymond et al.*, 1992; *von Breymann et al.*, 1992; *Torres et al.*, 1996; *Riedinger et al.*, 2006].

A recent study by *Serno et al.* [2014] casts doubt on the applicability of biogenic barite accumulation rates (as well as opal fluxes) for reconstructions of primary productivity or export production in the Subarctic North Pacific. Their preservation-corrected Holocene biogenic barium fluxes from 23 surface sediment samples throughout this area show weak and inconsistent correlations with published reference data for marine productivity and export production when being compared over regional scales. The authors do not preclude using biogenic barite as a qualitative proxy for changes in export production at a single location but strongly question the use of this method for quantitative and comparative purposes between different sites. As we are not attempting the latter and as our main findings do not depend on the proxy validity of biogenic barite, these findings are not critical here.

In order to differentiate the biogenic from the terrigenous barium components, many authors use Ba/Al or Ba/Ti ratios under the assumption that the relative proportions of terrigenous Ba, Ti, and Al fluxes are constant in space and time [Gingele et al., 1999; Reitz et al., 2004; Jaccard et al., 2010]. In our case, we opt for the XRF-CS based Ti counts as Ba normalizer (instead of Al) because of the better analytical precision of the XRF measurement for heavier elements [Tjallingii et al., 2007]. This makes no difference as the Ti and Al records of core SO202-39-3 are highly similar and show just minor discrepancies.

To verify the preservation potential of barite, pore water samples for sulfate analyses were taken soon after the recovery and opening of the core by means of rhizons, capillary soil moisture samplers, according to the procedure described by *Seeberg-Elverfeldt et al.* [2005] and *Dickens et al.* [2007]. Pore water sulfate concentrations were measured in 1:50 dilution using a *Metrohm Compact IC 761* ion chromatograph at the AWI in Bremerhaven.

4. Chronostratigraphy

4.1. Magnetostratigraphy and Cyclostratigraphy of Core SO202-39-3

With near absence of carbonate (mostly <2%) at depths below 4500 m, the available chronostratigraphic methods are magnetostratigraphy, tephrochronology, cyclostratigraphy, and diatom biostratigraphy. With sub-CCD North Pacific sedimentation rates of ~5–1 cm/kyr from west to east [Bleil, 1985; Hovan et al., 1991], our ~20 m long cores should have bottom ages of 400–2000 ka. Several previously published sediment chronologies of the abyssal North Pacific sediments were obtained by correlating their RPI records to global high-resolution RPI stacks [e.g., *Yamazaki*, 1999; *Yamazaki and Kanamatsu*, 2007]. A prerequisite for this approach is to identify and exclude magnetically overprinted sections.

Some rock magnetic properties of the magnetic carriers are therefore first introduced on a depth scale (Figure 2). All five magnetic parameters κ , Fe/ κ , ARM, ARM/IRM, and $S_{0.3T}$ alternate coevally between two distinct levels, which obviously represent two different sediment states. In the prevalent state (corresponding to lighter sediment colors), the magnetic concentration (κ , ARM), grain size (ARM/IRM), and mineral (Fe/ κ , $S_{0.3T}$) parameter values show typical mean values for oxic pelagic and abyssal clay sediments with minor variations. In the second state (corresponding to darker sediment colors, marked here by green shaded areas), a large

reduction of κ and disappearance of fine-grained magnetite (negligible ARM) is observed. Sharp magnetite grain size coarsening (reduced ARM/IRM) and a shift to a (relatively) more antiferromagnetic ($S_{0.3T}$) and paramagnetic (Fe/κ) petrology are strong indications for pervasive depletion of fine-grained magnetite, the expected NRM carrier. Such large and sharp signal shifts are commonly recognized as relict signatures of magnetite dissolution and known from many other marine records [e.g., *Leslie et al.*, 1990; *Hounslow and Maher*, 1999; *Itambi et al.*, 2009; *Hepp et al.*, 2009; *Just et al.*, 2012]. In these depleted sections, RPI data are of lower credibility and should not be used for dating according to established rules [e.g., *Tauxe*, 1993].

Outside the (coring-)disturbed 0–35 cm core top section, positive ($56.8^\circ \pm 7.2^\circ$) and negative ($-55.0^\circ \pm 6.8^\circ$) ChRM inclinations are stable and correspond well to the expected inclination of 57.4° of a geocentric axial dipole at 38°N (Figure 1). There is no discernable inclination shallowing suggesting that the sediment has not been compacted much since deposition. The only polarity reversal is the Brunhes/Matuyama boundary between 17.38 and 17.43 m, which was assigned an age of 778 ± 1.7 ka [*Tauxe et al.*, 1996]. Just below (17.63–17.73 m), the record shows the well-expressed Brunhes precursor excursion dated to 797 ka [*Roberts*, 2008]. The polarity excursion ($I = 6.3^\circ$) detected at 4.83–4.88 m in the Brunhes Chron is thought to represent the Iceland Basin excursion at 188 ka [*Roberts*, 2008].

A further age marker is the prominent tephra layer at 1.76–1.785 m, microscopically identified as the Aso-4 tephra [*Gersonde*, 2012]. This known event layer in MIS 5b, which is observed in many northwest Pacific records up to 2900 km east of the eruption center, the Aso Caldera on the South Japanese Island Kyushu, was dated to 86.8–87.3 ka [*Aoki*, 2008]. This and two other lithostratigraphically and magnetically prominent tephra layers at 13.82–13.87 m and 16.30–16.37 m (marked red in Figure 2) stand out by their high susceptibilities, low ARM/IRM ratios, and high RPI values. With linear interpolation of the previous age marks, these ashes possibly coincide with previously described Deep Sea Drilling Project (DSDP) Hole 810C tephras with stratigraphic correlation ages of ~ 590 ka and ~ 750 ka [*Natland*, 1993].

As expected, the RPI record shows low intensities at the Brunhes/Matuyama reversal and the three mentioned geomagnetic excursions. The bias of the RPI records in the dissolution layers is not strictly systematic, but in most instances, the signal is reduced. Over most parts of the RPI record, particularly the unaltered lower 11.35–19.00 m section, the signal patterns compare well to the NGC65/KR0310-PC1 North Pacific RPI composite [*Yamazaki and Kanamatsu*, 2007] and the global but “more Atlantic” RPI stack SINT-2000 [*Valet et al.*, 2005]. As Figure 3 shows, the mutual agreement of the two target records is good from 500 to 1000 ka, while they differ remarkably from 200 ka to 500 ka. The older part (> 500 ka) of the SOS202-39-3 RPI record can be easily correlated with either RPI target curve. Some uncertainty exists in the overprinted record section from ~ 860 to ~ 920 ka. The near-bottom RPI minimum at 19.98 m was correlated with the Santa Rosa geomagnetic event dated at 922 ± 4 ka by *Hong et al.* [2002]. The section-wise overprinted younger part (< 500 ka) of the RPI record has similarities with NGC65/KR0310-PC1, but the match is not as convincing as for the unaltered older part and remains methodically questionable.

To overcome dating uncertainties within this younger 0–500 ka section, the 1 cm resolution Ba/Ti record of SO202-39 was tied to the subarctic northwest Pacific Ba/Al record of Ocean Drilling Program (ODP) site 882 (Detroit Seamount, 3244 m water depth) [*Jaccard et al.*, 2010], one of the few available dated high-resolution sediment records in this area. Both records also match well in the magnetically dated older 500–800 ka section supporting our approach. The Ba correlation stratigraphy is also in accordance with the Aso-4 and Iceland Basin ages. Remaining age uncertainties of the target records and our correlations are thought not to exceed ~ 30 kyr. The resulting age-depth relation is relatively linear and yields a mean sedimentation rate of 2.14 cm/kyr.

4.2. Stratigraphic Correlation of SO202-39 to Cores SO202-38, -41, -42, -43, -44, and -45

The correlation of SO202-39-3 to six adjacent sediment cores of the same transect was established from stratigraphically consistent shipboard susceptibility logs (Figure 4). The plot shows two series of tie points, which can be followed over several cores. The “red series” encompasses nine tie lines (A–J) connecting isolated susceptibility peaks (in grey), which are clearly exceeding the usual plateau value (in brown) and were therefore associated with tephra layers. The “green series” comprises nine further tie lines (I–IX) linked to susceptibility minima, which usually descend to the assumed paramagnetic baseline value (light blue) and represent magnetite dissolution zones. The individual expression of both feature types varies from core to core, but the degree of consistency is considered sufficiently high to assume a quasi-isochronous nature. The westernmost

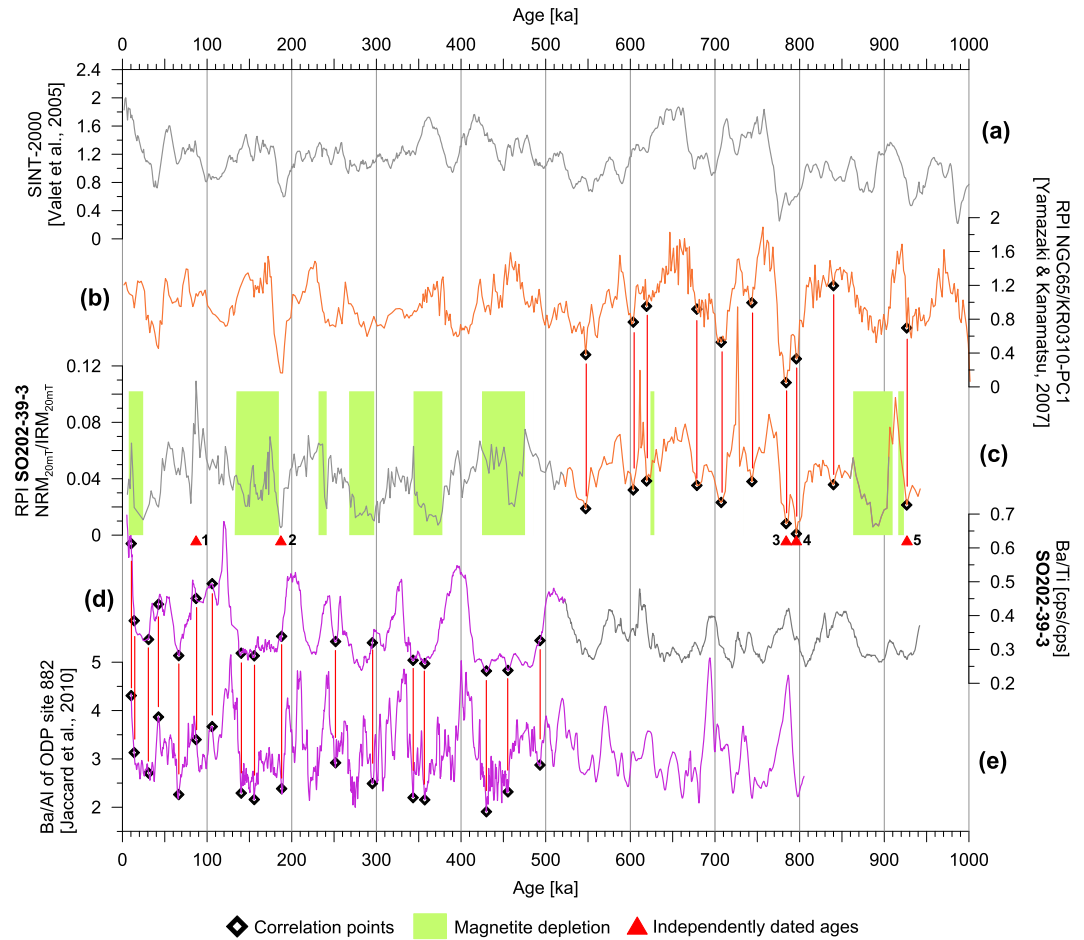


Figure 3. (c) Age model of core SO202-39-3 with relative paleointensity (RPI) record at center. Green bars mark zones of magnetite dissolution. Red triangles indicate ages from tephro- and reversal magnetostratigraphy (1—Aso-4 tephra, 86.8–87.3 ka [Aoki, 2008]; 2—Iceland Basin excursion, 188 ka [Roberts, 2008]; 3—Brunhes/Matuyama boundary, circa 778 ± 1.7 ka [Tauxe et al., 1996]; 4—Brunhes precursor excursion, 797 ka [Roberts, 2008]; and 5—Santa Rosa event, 922 ± 4 ka [Hornig et al., 2002]). The lower (brown) part of the RPI record was correlated to the (b) North Pacific RPI-stack of Yamazaki and Kanamatsu [2007]. The (a) SINT-2000 RPI stack of Valet et al. [2005] is shown to point out its good overall correlation to Figures 3b and 3c as well as some discrepancies. The upper part of the core, where the numerous magnetite dissolution zones question the fidelity of the RPI record, has been dated by tying its (d) Ba/Ti record to the dated (e) Site 882 Ba/Al record of Jaccard et al. [2010].

core SO202-45-1 could not be convincingly integrated into this stratigraphic network due to its numerous ash layers. The easternmost core SO202-38-2 instead shows less pronounced dissolution minima and obviously had the best preservation conditions for magnetite, possibly due to its lower sedimentation rate.

The averaged sedimentation rates (core length/bottom age) decline from west (4.5, 2.7, 3.0, and 2.9 cm/kyr) to east (2.14 and 1.9 cm/kyr) of the Shatsky Rise, reflecting increasing distance to Asian dust sources [Hovan et al., 1991; Yamazaki and Ioka, 1997]. For similar reasons, the frequency of identifiable tephra layers also decreases to the east. Likewise, the κ plateau values in unaltered section (brown) descend monotonously in steps of 600, 500, 450, 400, 300, and $250 \cdot 10^{-6}$ SI units from west to east accompanied by an equivalent decrease of κ dissolution minima (light blue threshold). Given that all cores have over 80% terrigenous content, the common case of increasing nonmagnetic (carbonate, opal) dilution with land distance does not apply here and source mixing and transport sorting need to be considered instead.

5. Proxy Records of Core SO202-39-3

The successful dating of core SO202-39-3 allowed us to compare the available multiproxy data in relation to glacial/interglacial cycles and middle to late Pleistocene transitions. We first show interrelations of various

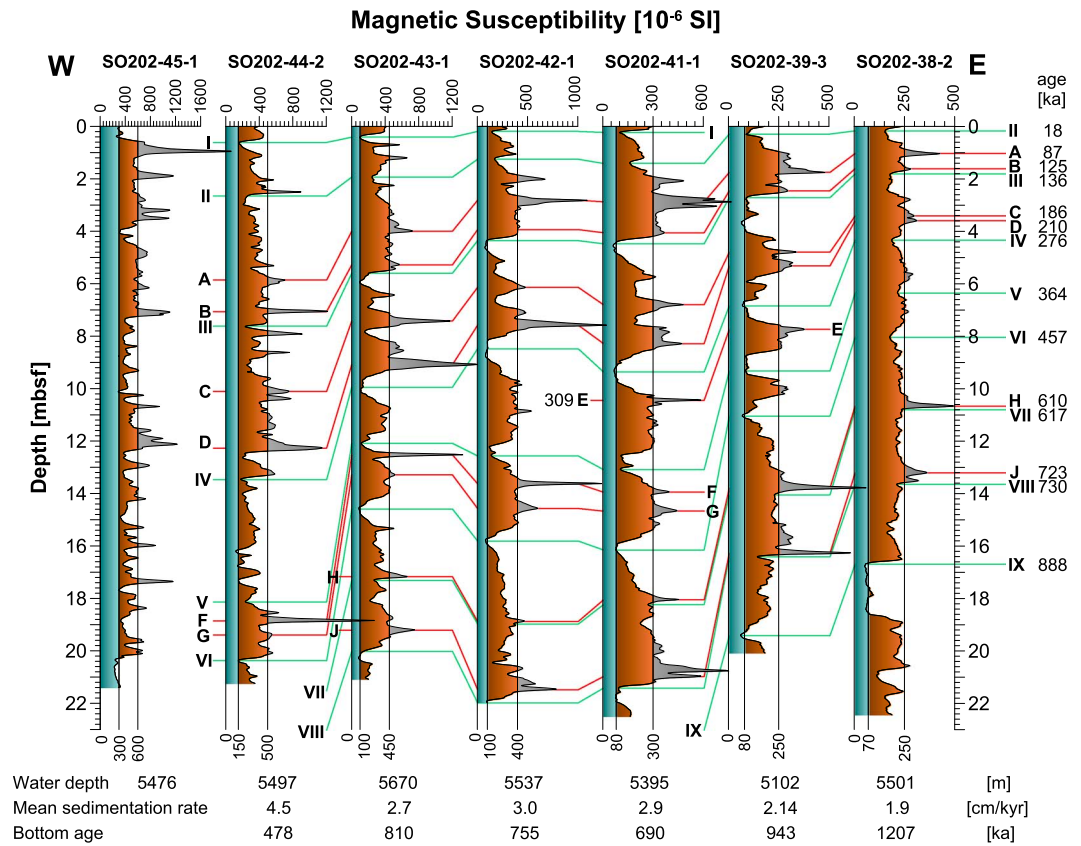


Figure 4. Correlation of shipboard magnetic susceptibility (κ) records of seven SO202 piston cores from the W-E northwest Pacific Basin transect (see Figure 1) versus depth. Peak values thought to correspond to tephra layers are interconnected by red lines and marked by letters. Minima associated with magnetite depletion are linked by green lines and labeled with Roman numbers. Tie line ages at right have been extrapolated from the SO202-39 age model. Light blue shaded areas indicate the paramagnetic portion of κ with a decreasing W to E (70 to 300) baseline level. Brown colors show ferromagnetic susceptibilities in unaltered sections, while grey spikes correspond to higher volcanic contents (tephra layers).

rock magnetic parameters to identify their proxy expression (Figure 5), look at the signatures and climate conditions of magnetite dissolution (Figure 6), and present further records of biogenic and terrigenous sedimentation (Figure 7).

5.1. Magnetic Mineral Assemblage and Magnetic Proxy Expression

In the following enviromagnetic approach, we identify magnetic minerals and their properties first by their contrasting multiparametric properties (Figure 5) as markers of dust, tephra, fluvial and glaciomarine input, authigenesis, and diagenesis before interpreting them in a stratigraphic context (Figure 6). Most magnetic source fractions are mineral mixtures whose properties vary with grain size and regional parent rock petrology. It is difficult to identify and quantify magnetic source or mineral fractions purely from their mixed magnetic properties. A magnetic provenance study would require a more representative sampling area, extensive electron microscopy, and a wider range of magnetic analytics. Such detailed petromagnetic studies of Pacific sediments were undertaken, e.g., by *Vali et al.* [1989] and *Yamazaki and Ioka* [1997]. According to their findings, the magnetic petrology of our North Pacific abyssal clays should primarily encompass three source fractions and one relict fraction: (1) terrigenous dust: moderately ferrimagnetic, hematite-rich, ~2–4 μm particles, (2) volcanic tephra: strongly ferrimagnetic, hematite-poor, 10–300 μm particles, (3) bacterial magnetofossils: ferrimagnetic, hematite-free, <<1 μm particles (chains), and (4) diagenetic relict facies: fine (<1 μm) ferrimagnetic inclusions, relict hematite.

Typical respective clastic particle sizes for the central North Pacific are from (1) *Rea* [1994], (2) *Natland* [1993], and (3) *Yamazaki and Ioka* [1997]. From the magnetic sources (1)–(4) above, we deduce that only (1) contributes to HIRM, (2) and, less, (1) contribute to $\text{IRM}_{20\text{mT}}$, and (3) plus submicrometer magnetic inclusions of all other fractions contribute to ARM.

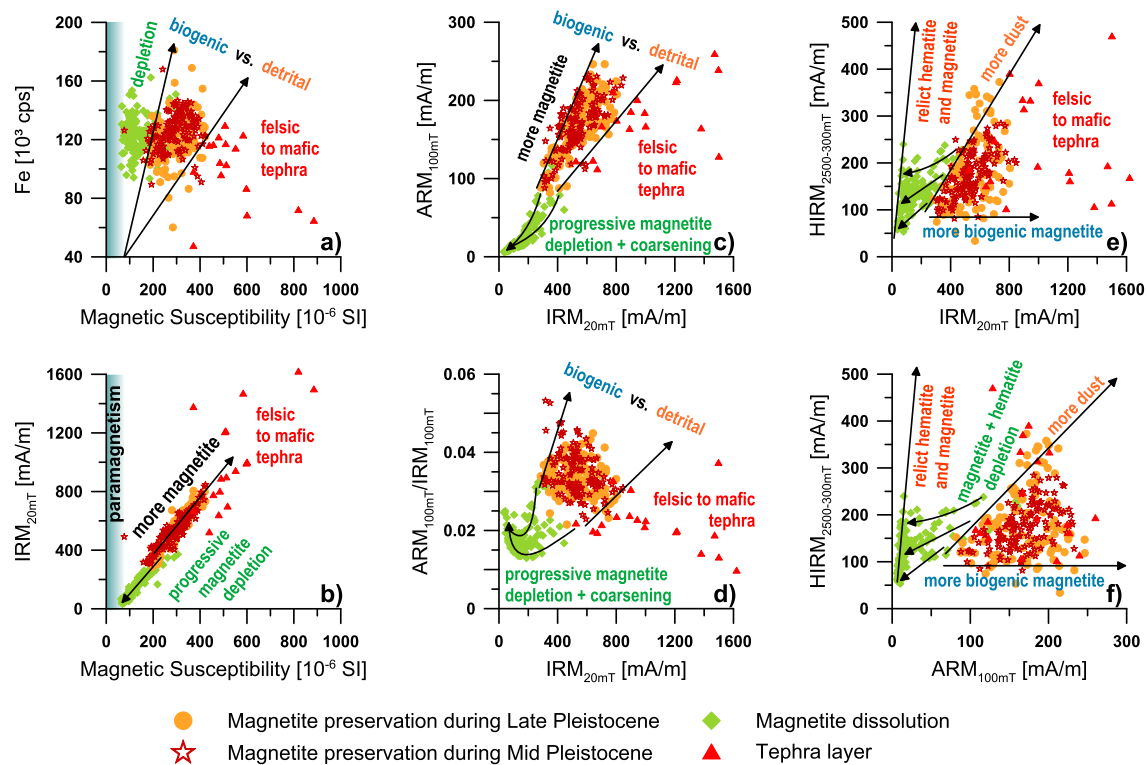


Figure 5. Rock magnetic proxy analysis of the SO202-39-3 core samples. Samples with high tephra content are characterized by high susceptibilities and rather high IRMs are marked as red triangles. Sediments without magnetite dissolution (orange circles and brown stars) contain varying mixtures of terrigenous (dust) and biogenic magnetic minerals, which do not differ before (brown) and after (orange) 500 ka. Samples from magnetite dissolution zones (green diamonds) are characterized by their low susceptibility, ARM, and IRM values and can be clearly separated from the unaltered sediment and tephra samples.

The four magneto-sedimentary fractions and their mixing regimes are depicted in Figure 5, where plot symbols of identified tephra layers are shown in red, unaltered mud in orange and brown, and altered (reduced) mud in green. From data groupings, three area-specific, plausible rock magnetic threshold criteria were defined to identify altered samples: $Fe/\kappa > 450$, $S_{0.3T} < 0.961$, and $ARM < 80 \cdot 10^{-3} \text{ A/m}$. The Fe versus κ plot (Figure 5a) shows a large 1:6 range of sediment susceptibilities from 70 to $400 \cdot 10^{-6} \text{ SI}$ ($300\text{--}900 \text{ idem} \cdot 10^{-6} \text{ SI}$ for ashes) contrasting to a much smaller 1:1.5 range of Fe contents ($\sim 9000\text{--}14000 \text{ cps}$ without outliers); obviously, most iron is not bound in a ferrimagnetic state. Altered samples have much lower and tephra samples far higher susceptibilities per Fe content. This allows us to define local oxic/suboxic boundary conditions for the Fe/ κ proxy. The IRM_{20mT} versus κ plot (Figure 5b) shows a close linear correlation of both parameters indicating that a varying accumulation of magnetite (dust) particles changes susceptibility κ from 200 to $400 \cdot 10^{-6} \text{ SI}$, while reductive dissolution of these particles drives κ below the oxic baseline at $250 \cdot 10^{-6} \text{ SI}$ down to the paramagnetic suboxic baseline of $70 \cdot 10^{-6} \text{ SI}$ (total magnetite dissolution except for inclusions). Tephra of varying composition is reflected by intense but widely scattered magnetic properties.

The ARM_{100mT} versus IRM_{100mT} plot (Figure 5c) shows considerably more scatter than Figure 5b due to the strong grain size dependence of ARM. Pure bacterial magnetite has higher ARM/IRM values ≥ 0.10 , while fine dust is around 0.02–0.04 [Schmidt *et al.*, 1999]. The data scatter with ARM/IRM ratios of 0.025–0.055 in Figures 5c and 5d implies that the sediment body is basically made up of fine dust, while bacterial magnetite is a variable additive. It is evident that all submicron magnetofossils disappear at the first onset of dissolution (little scatter below diagenesis threshold). A sharp drop of ARM is therefore a reliable indication, that iron-reducing conditions have been established in the sediment column. The curved track of progressive magnetite dissolution (Figures 5c and 5d) implies that only increasingly coarser detrital magnetite crystals can persist. The ARM/IRM versus IRM_{20mT} plot (Figure 5d) shows separate grouping of unaltered, altered, and volcanic facies. Interestingly, the ultimate relict facies has a nonzero ARM/IRM value of 0.015–0.02, equivalent to the respective ash value. This is due to the known fact that relatively small magnetic particles protected as inclusions within silicate host minerals [Hounslow and Maher, 1999; Alekseeva and Hounslow, 2004] and Ti-rich and therefore Fe(III)-poor Fe-Ti oxides

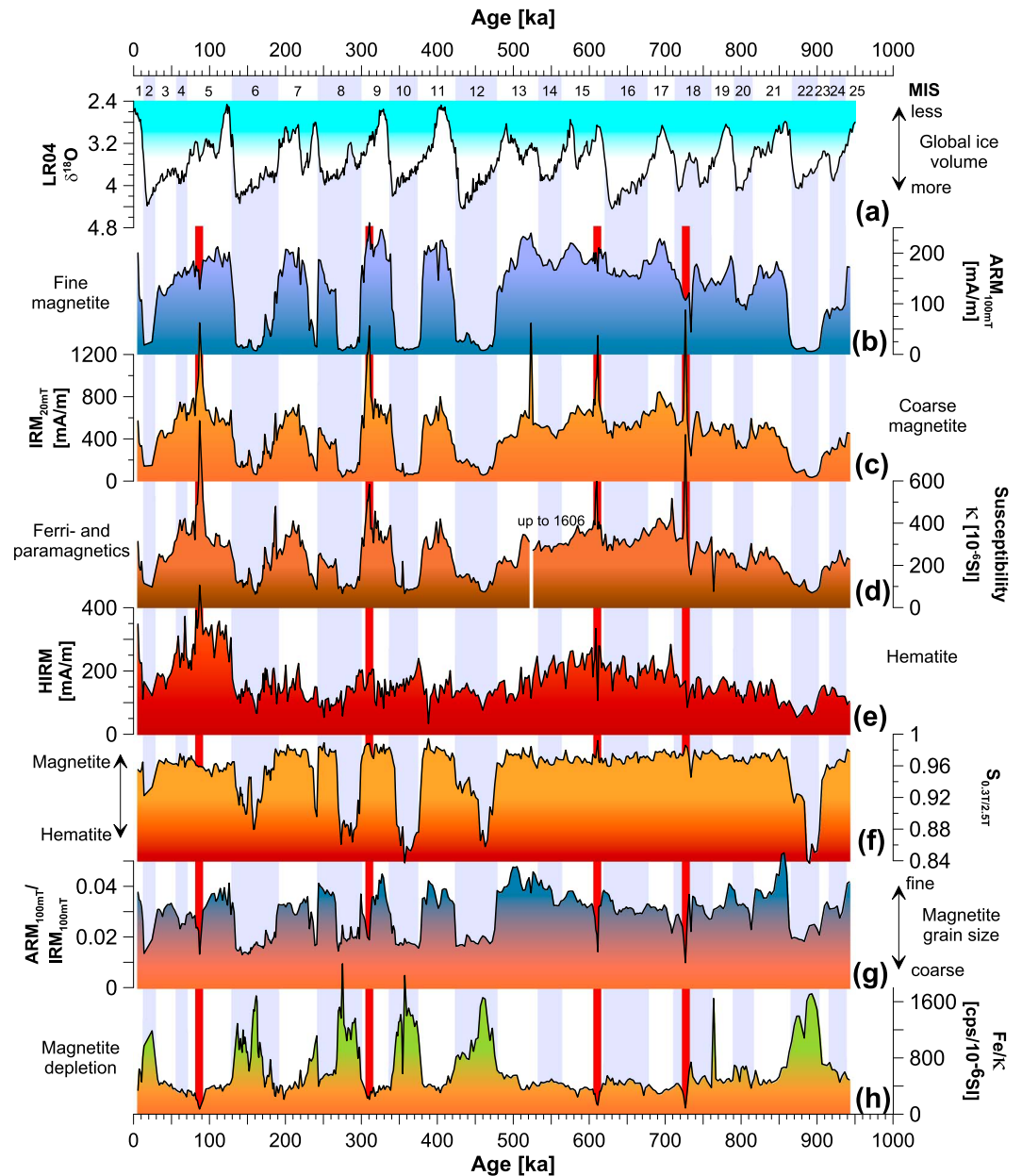


Figure 6. Selected magnetic parameters of core SO202-39-3 displayed versus age (see text). Marine isotope stages (MIS, glacial stages indicated by light blue bars) and (a) marine isotope stack LR04 [Lisiecki and Raymo, 2005] are given as paleoclimate reference. Depletion of fine magnetite and magnetic coarsening during glacial MIS 2, 6, 8, 10, 12, and 22 are observed in all magnetic records except for Figure 6e, whereas the glacial MIS stages 14–20 of the MPT show (b, c, h) minor or (f, g) absent signal shifts. Tephra layers are marked by red bars.

such as hemoilmenites [Dillon and Bleil, 2006; Dillon and Franke, 2009] can escape even pervasive reductive dissolution. Such inclusions and minerals are very common in volcanic ashes. Turning to the HIRM versus IRM_{20mT} plot (Figure 5e), we find that hematite is much less sensitive to reductive dissolution than magnetite (smaller HIRM loss versus higher IRM loss). This observation has been described by many previous studies [e.g., Robinson et al., 2000; Yamazaki et al., 2003; Liu et al., 2004; Emiroğlu et al., 2004; Garming et al., 2005]. The good distinction of unaltered and altered samples turns the S_{0.3T}/2.3T ratio into a mineral-magnetic diagenesis index here. The only moderate correlation of HIRM and IRM_{20mT} in unaltered sections suggests variations in dust composition such as different sources or weathering states. The final HIRM versus ARM plot (Figure 5f) spans a mixing model of terrigenous (HIRM) versus biogenic magnetite content with respective depletion tracks.

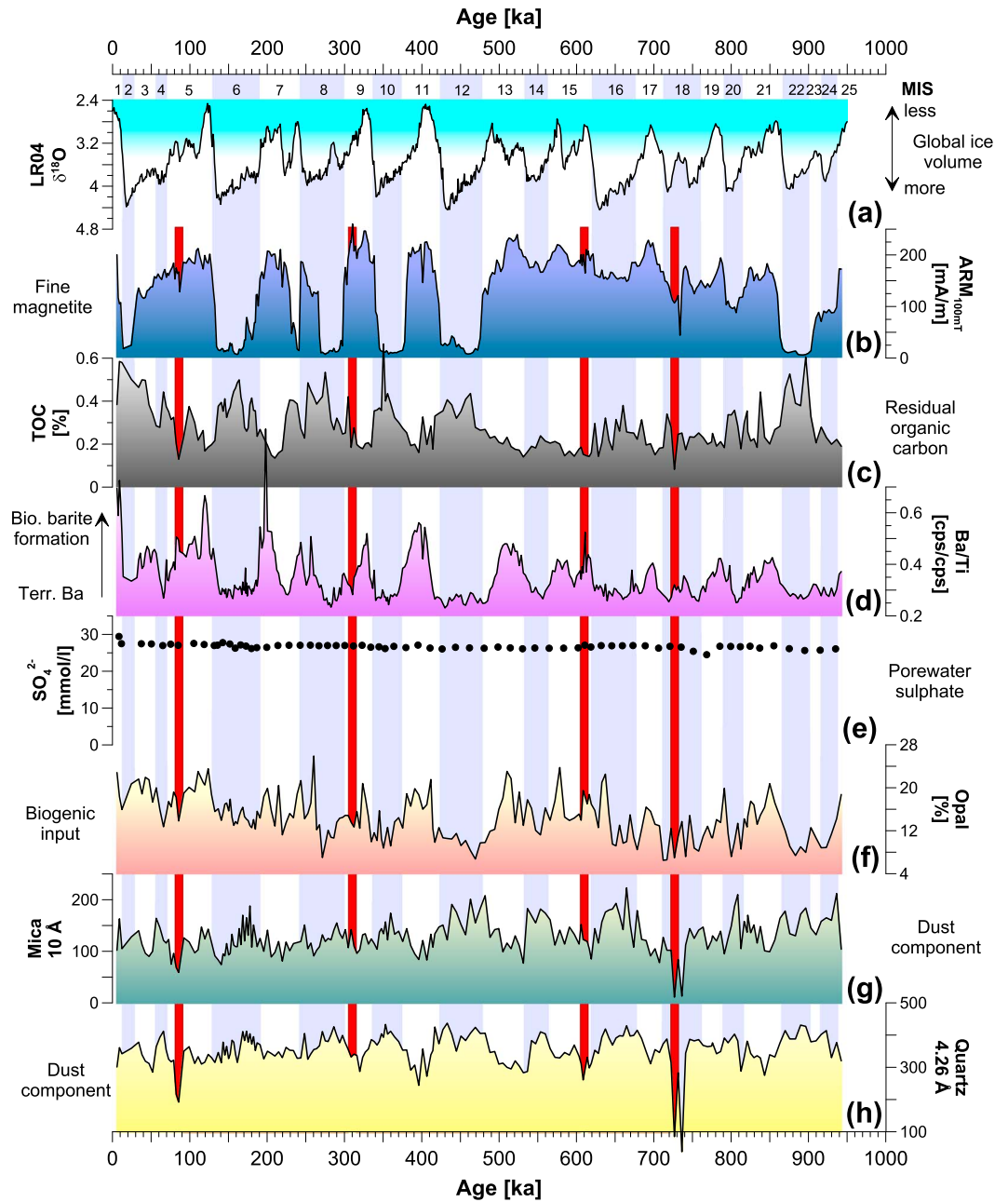


Figure 7. Selected geochemical and sedimentological parameters of core SO202-39-3 displayed versus age (see text). MIS (glacial stages indicated by light blue bars) and (a) marine isotope stack LR04 [Lisiecki and Raymo, 2005] are given as paleoclimate reference; (b) ARM marks magnetite depletion zones. (c) TOC represents the residual carbon content with highest values in magnetite dissolution zones. (d) Ba/Ti stands for organic carbon degradation in the water column. (e) Stable modern pore water sulfate suggests that no barite was mobilized. (f) Opal content mostly of diatomaceous origin shows that biogenic input has been higher during warmer stages, while (g) mica and (h) quartz concentrations indicate higher dust input during glacial times. Tephra layers are marked by red bars.

It can be concluded that rock magnetic parameters provide a clear and consistent view of the composition and differential dissolution of the sedimentary magnetic mineral inventory. Bacterial submicron magnetite particles of identical size are dissolved most rapidly after the establishment of suboxic conditions, identifying ARM as most sensitive parameter for absent bottom water oxygenation. Fine magnetite dust particles dissolve more slowly, while hematite (coatings?) and ferrimagnetic inclusions do not dissolve at all.

5.2. Climate Dependency of Magnetic Mineral Dissolution

To put reductive magnetite dissolution into a paleoclimate framework, all magnetic records of core SO202-39-3 are compared to the global marine $\delta^{18}\text{O}$ isotope stack LR04 of *Lisiecki and Raymo* [2005] (Figure 6a). All ARM dissolution minima coincide with glacial $\delta^{18}\text{O}$ maxima (Figure 6b). An apparently reverse climate correlation is observed from 270 to 230 ka, where magnetite is preserved in the late glacial MIS 8 and instead dissolved over a ~ 15 kyrs period in the early warm MIS 7. This narrow ARM trough seems to correspond to cold MIS substage 7.2 but is slightly offset. This feature may be an irregularity or a dating uncertainty, which does not show up in the two adjacent sediment cores (Figure 4).

The dissolution of bacterial magnetite during the cold MIS 22, 12, 10, 8, 6, and 2 (but not MIS 4) is pervasive down to the previously described minimum baseline of shielded magnetic inclusions (Figure 5d). During these middle to late Pleistocene glacial stages, the ARM record appears like a switching function, where fine magnetite dissolution turned on at an early glaciation stage and back off at the beginning of the deglaciation stage. In the section corresponding to mid-Pleistocene cold stages MIS 20, 18, 16, and 14, ARM is reduced by about 30%, but not flattened. This moderate ARM variability and even the amplitudes of $100\text{--}150 \cdot 10^{-3}$ A/m resemble glacial/interglacial ARM cycles of shallower Equatorial Pacific records published by *Yamazaki and Oda* [2005]. Whether these obviously climate controlled, but only gradual changes in fine magnetite content represent productivity, accumulation rates or light dissolution effects, remains open at this point. Moving to the $\text{IRM}_{20\text{mT}}$ record (Figure 6c) and the very similar susceptibility κ record (Figure 6d) we find comparable dissolution signals for dust-borne detrital magnetite during the same glacial stages as for ARM. The transitions between interglacial and glacial stages are more gradual and dissolution minima do not appear quite as flat and low. As shown before (Figure 5c), the much wider grain size and compositional variability of detrital lithogenic (as compared to biogenic) magnetic minerals leave room for a range of different reduction kinetics. Five narrow high spikes in both records identify magnetite-rich tephra layers.

The HIRM record (Figure 6e) should mainly reflect hematite and goethite content but may also be influenced by cation-substituted Fe oxides of intermediate coercivity (maghemite and hemoilmenite). HIRM shows a cyclic climate dependency only in the youngest MIS stages 1–5. Interestingly, the elevated HIRM values seen in the warm MIS 1 and 5 are not found in older interglacial periods. HIRM dissolution minima, e.g., within MIS 22, could suggest that two different high-coercivity mineral phases exist of which the first is robust and persistent (crystalline hematite?) and the second is more sensitive and hence more ephemeral in the lower part of the core (amorphous goethite?). As a result of the much lower variability of HIRM with respect to $\text{IRM}_{300\text{mT}}$, the $S_{0.3\text{T}}$ ratio preferentially reflects magnetite dissolution. Cyclic $S_{0.3\text{T}}$ records have been repeatedly interpreted as indication for changing eolian input to the deep North Pacific [*Doh et al.*, 1988; *Yamazaki and Ioka*, 1997; *Yamazaki*, 1999]. The $S_{0.3\text{T}}$ record of SO202-39-3 does not seem to bear much change in dust signature and remains almost constant over the full mid-Pleistocene period from MIS 21–13. The WE orientation and heavy alterations of the selected INOPEX cores are not ideal to track Asian dust and tephra provenance and we will keep our focus to postdepositional alteration. Some shallower, shore parallel INOPEX core transects hold more promise for provenance studies.

The $\text{ARM}_{100\text{mT}}/\text{IRM}_{100\text{mT}}$ record (Figure 6g), a magnetogranulometric ratio also used as a ventilation proxy by *Larrasoana et al.* [2003], follows the ARM dissolution cycles of Figure 6b. The surprisingly small change from ~ 0.04 down to only ~ 0.02 was already explained in the context of Figure 5d by the relatively high ARM/IRM ratio of the magnetic relict inclusions in silicate minerals. Ash layers form notches in the ARM/IRM record due to their much coarser magnetic particle size, similarly to the Fe/κ record (Figure 6h). Fe/κ and $S_{0.3\text{T}}$ stand out as mirror-like, equivalent dissolution records of the ferrimagnetic mineral fraction.

The coincident expression of all three diagnostic criteria (fine versus coarse magnetite, magnetite versus hematite, and ferrimagnetism versus paramagnetism) makes a very strong case for reductive magnetite dissolution in the abyssal northwest Pacific during glacial periods after and probably also before a strikingly different mid-Pleistocene phase from MIS 21 to MIS 13. It does not seem possible to explain such marked signals with terrestrial source changes or iron biomineralization.

5.3. Climate Dependency of Carbon Burial and Terrigenous Input

Potential drivers for pervasive glacial stage magnetite dissolution in the abyssal northwest Pacific are low bottom water oxygenation and/or burial of reactive organic carbon. Several driving factors must be considered: on one hand, a stronger stratification and lower ventilation of deep ocean basins due to changes in

thermohaline circulation, on the other hand, higher bioproductivity and more efficient export and preservation of organic matter (OM). We therefore present additional geochemical and sedimentological records of core SO202-39-3 as evidence for changes in the productivity, export, and preservation of organic carbon. Higher terrigenous input can also actively enhance nutrient supply, scavenging, and carbon burial.

We use again the LR04 $\delta^{18}\text{O}$ stack as climate signal (Figure 7a) and SO202-39-3 ARM as the most sensitive and indicative of all shown magnetic depletion parameters (Figure 7b). Sedimentary TOC content (Figure 7c) is relatively low ($\sim 0.15\text{--}0.2$ wt %) in all the unaltered interglacial sections. It is higher ($\sim 0.4\text{--}0.6$ wt %) in the younger glacial sections with magnetite dissolution and just slightly enhanced (~ 0.3 wt %) in the mid-Pleistocene glacial sections. Biogenic magnetite appears to remain stable in sections with TOC levels ≤ 0.25 wt % and is fully dissolved at TOC levels at ≥ 0.4 wt %. Interestingly, exactly the same TOC thresholds were observed for pelagic Equatorial Atlantic records [Funk *et al.*, 2004a]. The residual organic carbon phase apparently does not react with Fe(III) and not even with O_2 , as elevated TOC values of 0.6 wt % at 20 cm sediment depth (MIS 2) suggest. If reactive TOC was buried under glacial conditions within Fe(III)-depleted zones, it should not have survived the O_2 burn down during the subsequent deglaciation. It is therefore reasonable to assume that all preserved TOC is of non-reactive character. The glacial-interglacial TOC changes during cold MIS 22, 12, 10, 8, 6, and 2 (0.4–0.6 wt % versus 0.15–0.25 wt %) correspond to a variation factor of 2–3. Given that the (diluting) eolian background sedimentation rates were also some 2–3 times higher during the LGM than during the Holocene [Rea, 1994; Kohfeld and Harrison, 2001; Balsam *et al.*, 2005; Shigemitsu *et al.*, 2007], the accumulation rates for (nonreactive) organic carbon must have been $\sim 4\text{--}6$ times higher during glacial periods to produce the observed glacial TOC concentrations.

It is an obvious question whether these varying TOC fluxes into the sediment reflect higher productivity, more efficient transport, and/or better preservation of organic carbon. Opal content (Figure 7f) and Ba/Ti (Figure 7xd) are commonly used but quite controversial proxies for paleoproductivity [Zonneveld *et al.*, 2010]. A precondition for the long-term conservation of biogenic barite is permanent absence of sulfate depletion [Torres *et al.*, 1996]. Constant sulfate pore water concentrations of >26 mmol/L over the full core (Figure 7e) seem to support barite stability under present conditions. In published records from the subarctic northwest Pacific [Jaccard *et al.*, 2010], both opal and Ba/Ti show systematically higher values for warmer climate stages, implying that bioproductivity and carbon export from the photic zone were at their “maximum efficiency” [Jaccard *et al.*, 2010] during interglacial stages. The flat Ba/Ti minima of core SO202-39-3 during glacial stages possibly mark the lithogenic Ba baseline. They imply either far lower organic matter fluxes and/or widespread suboxic conditions in the water column limiting barite formation in sinking aggregates.

The anticorrelations of TOC and both (under ruling conditions uncertain) productivity proxies suggest that organic carbon accumulation and bioproductivity were decoupled during glacial conditions. Lower or absent oxygen content in the glacial NPDW would considerably reduce the modern $\sim 97\%$ recycling rate of POM [e.g., Martin *et al.*, 1987] during its descent from the surface ocean (100 m) into the deep North Pacific (5000 m). Under modern oxic conditions, benthic organic carbon degradation in the benthic boundary layer remineralizes another $\sim 98\%$ (abyssal) of the effectively settled POM [Hartnett *et al.*, 1998], where the net burial rate depends mainly on “oxygen exposure time.” This major carbon loss after settling would have been inhibited in the hypothetical case of near absence of dissolved oxygen (and nitrate) in glacial bottom water. A likely third clue is more rapid and efficient organic carbon transport via scavenging by enhanced and coarser glacial dust falls. Such higher glacial dust fluxes are documented by larger terrigenous contents (from 80% to 90%, see Figure 7f). Higher quartz and mica contents (Figures 7g and 7h) coincide with higher dust grain sizes. We speculate that quicker sinking of large agglomerates of detrital and organic matter after dust outbreaks would have reduced organic carbon decomposition in the oxygenated upper water column.

6. Paleooceanographic Implications of Carbon Trapping and Magnetite Dissolution

6.1. Multiproxy Perspective at a North Pacific 100 kyr Ice Age Cycle

The observed glacial stage magnetite depletion zones in the abyssal northwest Pacific Ocean appear to have partaken in a climatic process chain driven by Milankovic cycles. The coupling of POM oxidation with magnetite reduction ties the rock magnetic proxy records to Northern Hemisphere glaciation and global carbon cycles. The 220–120 ka section of SO202-39-3 proxy records (Figure 8a) exemplifies the characteristic sediment response to a 100 kyr ice age cycle, which coincides with periodic insolation changes and is mediated by sawtooth-type variations in atmospheric greenhouse gas concentrations (EPICA CO_2) and global ice volume (benthic $\delta^{18}\text{O}$).

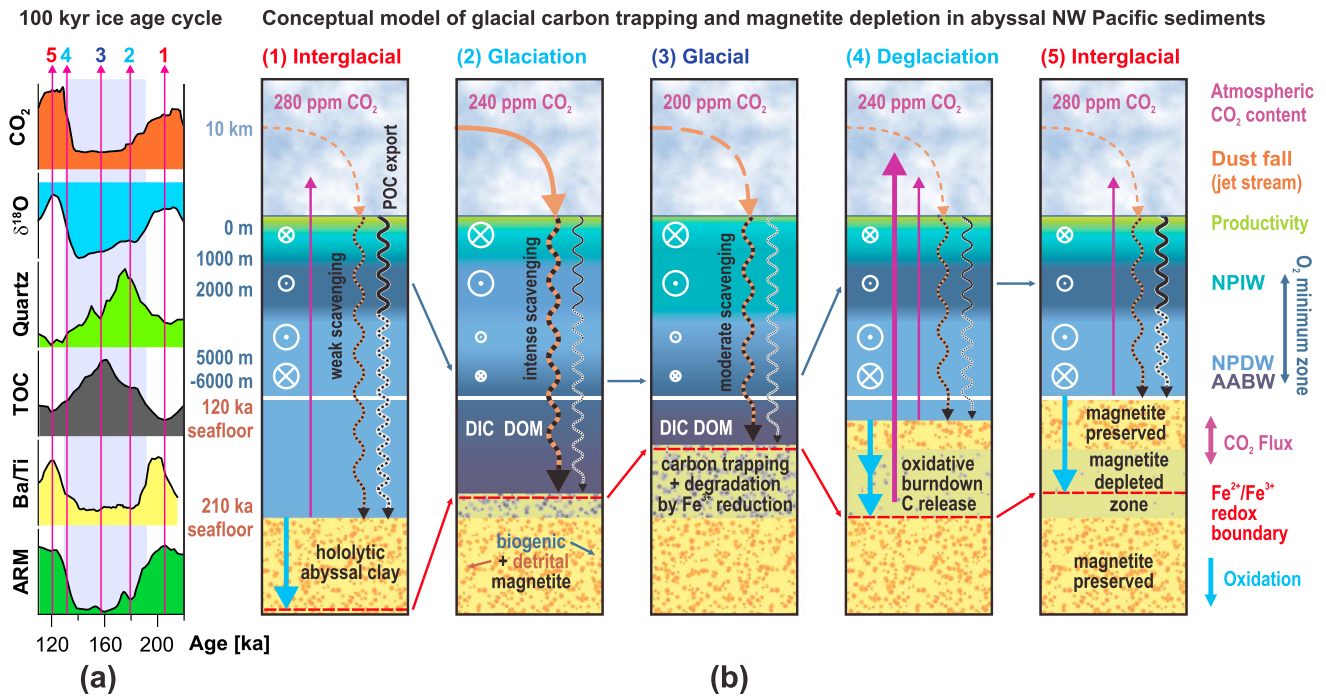


Figure 8. (a) Compilation shows indicative parameter changes during an exemplary 100 kyr cycle from interglacial MIS 7 (Figure 8b1) over glacial MIS 6 (Figure 8b3) into interglacial MIS 5 (Figure 8b5) with highlighted interglacial periods (1, 5), glaciation (2), full glacial (3), and deglaciation (4). (b) Columns 1–5 represent a conceptual model of glacial carbon cycling and magnetite depletion in abyssal NW Pacific sediments over the five situations marked in Figure 8a. Changes in atmosphere (CO₂, dust input) and ocean conditions (productivity, O₂ minimum, current strengths, scavenging, and DIC + DOM content) entail glacial sedimentary carbon trapping, zonal magnetite depletion, and rapid deglacial CO₂ release. The glacial atmospheric CO₂ change depicted in Figure 8a is shown for reference and not as a direct result of the above depicted carbon capture process. The meaning of arrows is explained on the right side panel or in the plots. White circles represent northward (cross) and southward (dot) current directions where symbol size stands for current intensity.

The quartz and (residual) TOC records of Figure 8a show relatively symmetric triangular cycles. Quartz content peaks with known enhanced dust flux from Asia during early glacial stages [Hovan *et al.*, 1991; Rea, 1994], enabling a more efficient POM transport to the seafloor by scavenging mechanisms. The TOC peak lies within the midglacial period, when NW Pacific bottom water oxygenation may have reached its minimum according to our scenario. Under the premise that suboxic or even anoxic sediment conditions enabled an additional, proportionally higher burial of reactive organic matter, which was remineralized and released during deglaciation, the relict TOC record (Figures 7c and 8a) should underestimate the original glacial TOC content in the sediment subsurface by far.

The Ba/Ti pattern is clearly anticyclic with TOC; it features steep symmetric triangular maxima in interglacial stages and flat baseline minima during glacial stages. According to Jaccard *et al.* [2010], Ba peaks link to nutrient-controlled interglacial productivity maxima. However, as the formation and input of barite to the sediment is assumed to be controlled by aerobic decay of TOC in the water column, glacial barite formation could have been lowered by quicker sinking (ballasting) and shorter exposure to oxygenated water layers. Both factors reduce carbon remineralization and biogenic barite formation during descent and at the sediment surface. We conclude that the benthic carbon degradation efficiency should have been at minimum during glacial periods.

The characteristic generalized waveform of submicrometer magnetite content (ARM) is rectangular (Figure 8a) where zones of total depletion fall into glacial stages. The steep flanks toward preservation coincide with early glaciations and early deglaciations. More than other presented records, the preservation or dissolution of bacterial magnetite (which is formed by microaerophilic microbes in the subsurface sediment) is a nonsteady state process, where the reaction of organic carbon with fine-grained Fe₃O₄ in the surface sediment is on and off according to changing bottom water oxygenation and resulting redox conditions in the subsurface sediment, where magnetotactic bacteria live. One may ask, which pore water conditions are actually required to sustain bacterial magnetite biogenesis. As magnetotactic bacteria are an ancient microaerophilic species

adapted to nearly O₂-free early Earth conditions [Chang and Kirschvink, 1989], they are commonly found even in poorly ventilated aquatic environments [Bazylinski et al., 1991]. Magnetite biomineralization should therefore persist even under suboxic glacial conditions; however, magnetosomes will not be fossilized then.

6.2. Conceptual Process Model for Glacial Carbon Trapping and Release

The above described interrelations and feedbacks can be formulated as a simplified conceptual process model (Figure 8b). Alternating glacial-interglacial conditions are provided by the anticyclic ventilation changes of the North Pacific Intermediate and Deep Water bodies [Jaccard and Galbraith, 2013]. Starting in a well-ventilated interglacial world (Figures 8b–81), our exemplary ice age cycle is set off by a (initially insolation driven) slow down of meridional overturning circulation in the deep Pacific. The closure of the Bering Strait at falling sea level enhances NPIW formation [Knudson and Ravelo, 2015]. In the early glaciation stage, a still oxic benthic redox environment is exposed to northward expanding, increasingly stagnant, oxygen-depleted, and CO₂-saturated AABW-sourced bottom water (Figure 8b2). Downward oxygen diffusion is no longer replenished from above and sedimentary reservoirs are rapidly consumed. This shifts the interglacial iron redox boundary from an estimated 1–2 m sediment depth to near the sediment-water interface. The burial and accumulation rates of reactive POM increase dramatically since organic carbon degradation with mineral-bound Fe(III) is much slower and energetically less favorable compared to aerobic remineralization. The very fine grained bacterial magnetite is firstly and irreversibly consumed as electron acceptor for organic carbon remineralization. As the glacial period evolves further (Figure 8b3), the magnetically depleted layer widens.

At the glacial termination (Figure 8b4), the deep ventilation of the Pacific is reactivated [Okazaki et al., 2010, 2012] and newly arriving oxygen diffuses into the suboxic sediment, burning off the trapped reactive carbon [e.g., Thomson et al., 1984; Wallace et al., 1988; Kasten et al., 2001] and releasing an intense CO₂ flux out of the sediment into the bottom water from which it can later escape to the atmospheric pool. Higher glacial TOC levels and a prominent depletion in iron oxide minerals remain permanent signatures of suboxic glacial redox conditions (Figure 8b5). Secondary minerals formed by reoxidation of Fe²⁺ are generally amorphous and paramagnetic [Hounslow and Maher, 1999]; they do not contribute to magnetic remanence parameters.

6.3. Storage Capacity and Reservoir Age of the Sedimentary Carbon Pool

As argued above, sediments deposited in a low-oxygen glacial NW Pacific abyss must have experienced much lower benthic OM degradation losses. In the well-ventilated Pacific basins of today, low sedimentation rates and good oxygenation result in the lowest known benthic OM preservation rates of ~0.001–0.01%, while hundredfold higher rates of ~0.1–1% occur in low-oxygen zones of the East Pacific margin [Bralower and Thierstein, 1984]. Under anoxic bottom water conditions, carbon burial is entirely decoupled from sedimentation rate and controlled by microbial turnover. We can speculate how high glacial TOC contents in the glacial subsurface of our area may have been by looking at modern TOC values in East Pacific oxygen minimum zones. Hartnett et al. [1998] published values of 0.5–2.8 wt % TOC for the oxygen-poor (38–104 μmol/L O₂) Washington slope and 7.5–12.8 wt % TOC for the almost oxygen-free (0–12 μmol/L O₂) Mexican slope.

To provide a rough estimate for NW Pacific glacial carbon trapping capacity under suboxic conditions, we assume a 2 wt % surplus TOC burial (i.e., a total of ~2.5 wt % TOC), 2 cm/kyr sedimentation rate, 2.5 g/cm³ grain density, 80% sediment porosity, and 50 kyr ice age duration. These numbers yield a cumulative temporary glacial organic carbon deposit of ~10 kg/m². If we delineate the abyssal northwest Pacific space below 4500 m with ~3 · 10¹² m², this translates into glacial sedimentary carbon trapping of 30 Pg C. The 200–280 ppm glacial-interglacial atmospheric CO₂ change corresponds to ~170 Pg C [Sigman and Boyle, 2000] and the estimated carbon storage capacity therefore appears as irrelevant. Extrapolating the 10 kg/m² glacial carbon storage capacity to the entire abyssal Pacific Ocean delivers a cumulative release of ~650 Pg C, which is a more relevant number. But without local evidence, such ocean-wide extrapolations are highly questionable considering the varying POM fluxes and burial rates of different deep Pacific Ocean basins.

According to estimates, the global DIC and DOM pools of the deep oceans are as large as 38,000 Pg [Sigman and Boyle, 2000] and even small temperature-driven changes of this vast mass outnumber by far the temporary carbon trapping capacity of the volumetrically much more constrained abyssal surface sediment. Still, POM residence time in the sediment could be as long as a full glacial period, i.e., much longer than the deep water DIC reservoir age, which is thought to be in the order of 1250 kyr. Providing an additional rapid CO₂ release during deglaciation, the sedimentary carbon pool can possibly

play a role for deglaciations as positive feedback mechanism. Originating from ^{14}C -dead POM, this sudden sedimentary CO_2 release should have evoked reversed ^{14}C ages of benthic microfossils, which has been observed elsewhere under comparable conditions [Broecker *et al.*, 2004; Hain *et al.*, 2011] but could not be measured here because of the negligible carbon content and missing carbonate.

6.4. Spatiotemporal Variability of Sedimentary Magnetite Depletion Patterns

A local driver of the depicted nonsteady state redox process is sedimentation rate. Higher terrigenous background sedimentation enhances carbon burial efficiency and retards the postglacial carbon burn down. NW Pacific susceptibility records in greater proximity to Asia and hence with higher dust accumulation show more frequent and more complete magnetite dissolution features (Figure 4). Signal characters and widths of corresponding dissolution layers seem to vary from core to core, underlining that the geochemical zonation in the subsurface varies with local sedimentation conditions. For example, the susceptibility troughs between tie lines III and IV (MIS 6 and 8) become increasingly deeper toward the adjacent western core sites SO202-41, -42, and -43 and are shallower at the eastern site SO202-38. The two westernmost cores show spikier and more complex records due to the many tephra layers intermitting the background sedimentation. The easternmost core SO202-38-2 (5501 m) experienced only partial magnetite dissolution throughout all cold stages before 900 ka, which could at least partly result from its low mean sedimentation rate of 1.9 cm/kyr. Core SO202-42-1 is from comparable depth (5537 m) but farther west; its mean sedimentation rate of 3.0 cm/kyr is 60% higher, and accordingly, it suffered pervasive magnetite dissolution during almost every glacial stage. Obviously, higher sedimentation rates facilitate glacial magnetite depletion.

Another environmental factor is local bottom current intensity, which depends on seafloor topography and the location of deep water passages. Under conditions of a very sluggish bottom circulation, benthic oxygen minimum zones should preferentially develop in topographically sheltered zones with nearly stagnant laminar flow and minimum vertical mixing. The resulting lateral variability in bottom water O_2 depletion should be mirrored in sedimentary redox conditions.

6.5. Deep Pacific Ventilation During and After the Mid-Pleistocene Transition

The mid-Pleistocene transition (MPT) at around 900 ka marks a climate system change from an obliquity- (41 kyr world) to an eccentricity-dominated (100 kyr world) ice age cyclicity [Maasch, 1988; Raymo *et al.*, 1997; Mudelsee and Schulz, 1997; Diekmann and Kuhn, 2002]. At the same time, CaCO_3 records from Atlantic and Pacific sectors reverse their correlation from in phase to antiphase [Sexton and Barker, 2012]. SO202-39-3 stretches over the past 960 kyr and covers this entire global cooling period (Figures 9a and 9b). It is interesting to note that MIS 22 (900–865 ka), the first “real” 100 kyr cycle beside precursor MIS 34 [Schmieder *et al.*, 2000], corresponds to an incisive early magnetite dissolution event recorded by all our cores, even the otherwise unaffected westernmost core SO202-38-2.

Little or no magnetite dissolution occurred during the following mid-Pleistocene glacial stages MIS 20, 18, 16, and 14 (815–530 ka) (Figures 6b, 6f, and 6h). Our rock magnetic data indicate that the abyssal northwest Pacific was much better oxygenated during these cold stages of the MPT than during the subsequent cold stages MIS 12, 10, 8, 6, 4, and 2. Figure 5 differentiates data with magnetite preservation into syn-MPT (>500 ka, brown) and post-MPT (<500 ka, orange) categories. The overlap of both subgroups suggests that the magnetic mineral composition did not vary much through time. Conditions for glacial magnetite preservation (and therefore the oxygenation conditions) were however far better during the MPT than after the establishment of regular 100 kyr cycles (Figure 9b).

Mills *et al.* [2010] studied the distribution of redox-sensitive metals in metalliferous hydrothermal plume fallout deposits at the southern East Pacific Rise and identified uranium and manganese precipitation layers which mark one active and three relict oxidation fronts. These fronts were only found within (U), respectively, above (Mn) MIS 12, 10, 8, and 6 (very faintly also in MIS 2) but are absent in older glacial sections (Figure 9c). The authors’ hypothesis of a basin-wide deep Pacific ventilation at glacial-interglacial terminations since 500 ka agrees well with our findings. Their core is from shallower water depth (3044 m) than ours and also from much farther south ($14^\circ 47.9'S$, $113^\circ 30.1'W$). It is not clear how the vertical reach of suboxic bottom water conditions at this site relates to the northwest Pacific.

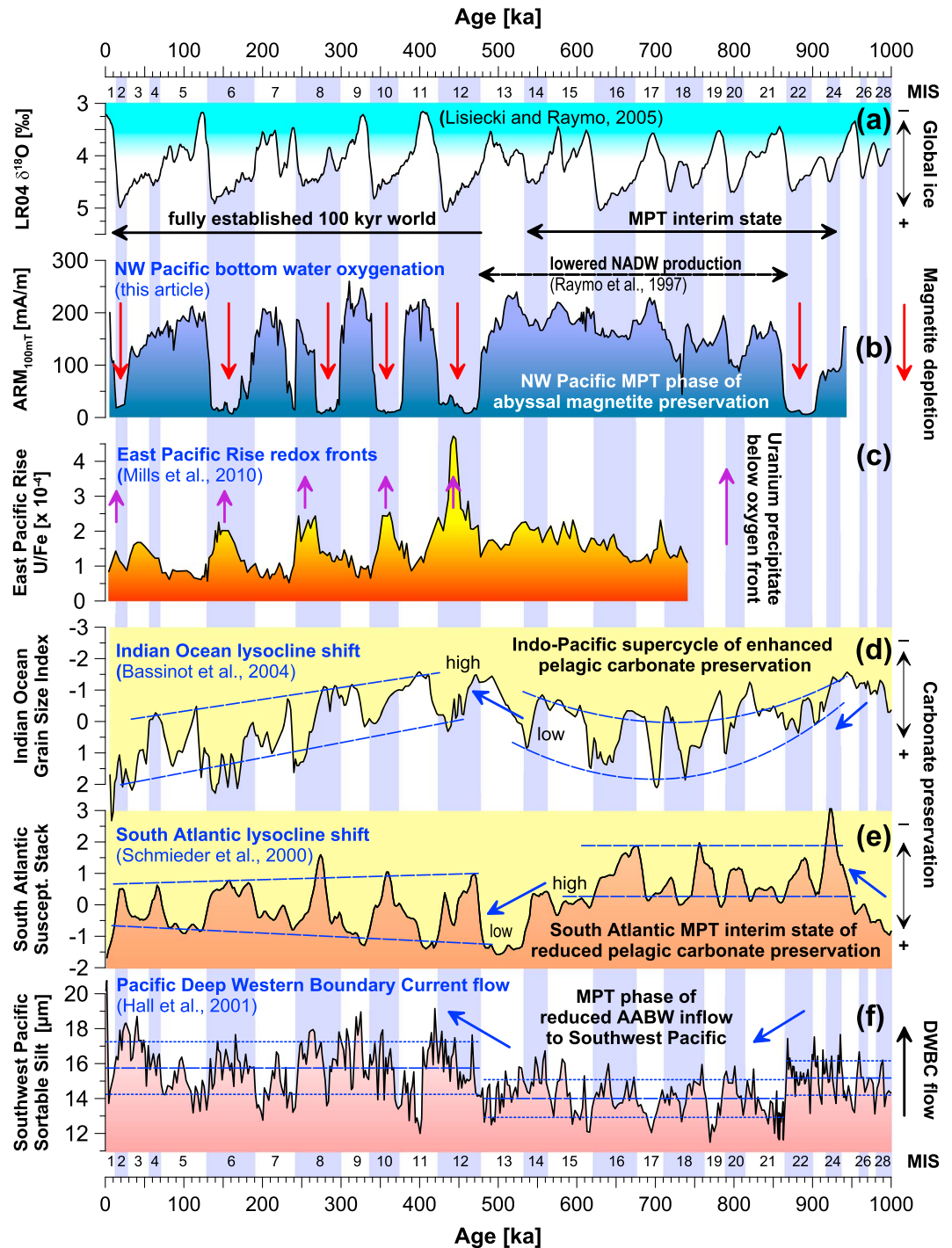


Figure 9. Comparison of core SO202-39-3 with published records for deep ocean ventilation. (a) Marine isotope stack LR04 by *Lisiecki and Raymo* [2005] is given as paleoclimate reference; (b) ARM lows mark magnetite-depleted zones (red arrows) and coincide with uranium precipitate layers (purple arrows) from repeated deglacial oxygen burn downs of a metalliferous (c) East Pacific Rise core [Mills et al., 2010]. (d) The Indian Ocean Grain Size Index by *Bassinot et al.* [1994] and (e) the Subtropical South Atlantic Susceptibility Stack by *Schmieder et al.* [2000] signalize anticorrelated glacial lysocline shifts in both basins, which suggest a change in AABW partitioning between Atlantic and Indo-Pacific sectors. (f) The mean sortable silt size at ODP Site 1123 east of New Zealand [Hall et al., 2001] indicates reduced AABW flow into the SW Pacific Ocean between MIS 21 and MIS 13. Dashed and dotted lines mark means and standard errors for the periods from MIS 28 to MIS 22, MIS 21 to MIS 13, and MIS 12 to MIS 1.

Schmieder et al. [2000] concluded from pelagic South Atlantic susceptibility records controlled by carbonate accumulation changes that the MPT interim state from 920 to 540 ka experienced a vertical expansion of LCDW in the deep South Atlantic (Figure 9e). The resulting upward shift of the glacial CCD considerably reduced calcite preservation in the deep South Atlantic and thereby enhanced the magnetic susceptibility of the carbonate-depleted pelagic sediments. This period corresponds largely to a high in the Indo-Pacific supercycle of pelagic carbonate preservation [*Bassinot et al.*, 1994] (Figure 9d), which points at better bottom water ventilation in this sector before the Mid-Brunhes Event (MBE) from MIS 15 to MIS 11 with higher carbonate dissolution.

There is also sedimentological evidence [*Hall et al.*, 2001] from ODP Site 1123 (3290 m depth, middle CDW) and environmental magnetic evidence [*Venuti et al.*, 2007] from Site MD97-2114 (1935 m depth, upper CDW), both situated at the NE slope of New Zealand's Chatham Rise, that the DWBC experienced unusually low bottom current velocities between MIS 21 and MIS 13 (Figure 9f). Both studies take changes in the glacial production of AABW associated with polar sea ice sheets responsible for variations in the deep Pacific Ocean inflow during the MPT interim phase. As pointed out by *Jaccard and Galbraith* [2013], this flow did not seem to reach the abyssal North Pacific.

Cyclic glacial magnetite depletion in the abyssal northwest Pacific started in MIS 12 after the MPT phase from MIS 21 to MIS 13 and points to an expansion of ultracold and saline AABW over the previously described choke points into the abyssal northwest Pacific. This northward glacial expansion into the Indo-Pacific sectors in MIS 13 could be the consequence of a coeval retreat in the Atlantic sector. A driving factor of LCDW/AABW partitioning between oceans could be the shift from a significantly lower North Atlantic Deep Water (NADW) production from MIS 21 up to MIS 12 [*Raymo et al.*, 1997] to a larger NADW production from thereon.

Several studies have compiled and compared MPT records of different origin and nature [e.g., *Wang et al.*, 2003, 2004, 2014] and no holistic explanation has yet been presented to explain all phenomena. There is debate whether the MPT climate shift was primarily driven by the 400 kyr eccentricity supercycle, the so-called "heartbeat of the Oligocene" [*Pälike et al.*, 2006] and other Neogene periods [e.g., *Wang et al.*, 2003, 2004, 2014], or by a quasi-cyclic ~500 kyr adjustment of the cooling Pleistocene climate system. Whether such an adjustment should be considered as a "contrasting state of the Pleistocene global circulation system with reduced NADW formation and weaker deep water exchange between Atlantic and Indo-Pacific" [*Schmieder et al.*, 2000] or rather as a "slightly irregular cycle" resulting from the distortion of a 400 kyr supercycle by discrete events [*Bassinot et al.*, 1994] is still an open issue to which our new records and compilations contribute within their limited age frame. There is a clear need for longer abyssal NW Pacific records to see, how far back in time the glacial abyssal magnetite depletion process existed and if was synchronous with other known 400–500 kyr supercycles of the Pacific [*Wang et al.*, 2004].

7. Conclusions

The magnetic susceptibility records of a piston core transect across the abyssal northwest Pacific show largely consistent cyclic glacial magnetite dissolution zones and episodic tephra spikes. The conclusive geomagnetic polarity and paleointensity patterns of the master record SO202-39-3 imply continuous sedimentation since 960 ka at a mean rate of 2.1 cm/kyr. Rock magnetic analyses confirm that all authigenic bacterial and most lithogenic eolian magnetite in the glacial sections of "100 kyr" MIS 22, 10, 8, 6, 4, and 2 has been irreversibly dissolved, while it largely survived in the glacial sections of MIS 20, 18, 16, 14, and 12 during the MPT interim phase. In all interglacial sections, however, the detrital and the delicate submicron bacterial magnetite fraction are remarkably well preserved. Such abrupt shifts in sedimentary mineral content cannot be explained with source changes or transport effects and must result from large changes in preservation conditions, i.e., the abyssal redox environment.

Ferric iron contained in magnetite, hematite, goethite, and other paramagnetic iron minerals is a preferential electron acceptor for organic carbon remineralization in the absence of oxygen and nitrate. The magnetically depleted zones evidence oxygen depletion in the glacial northwest Pacific bottom water below 4500–5000 m water depth. A coeval rise in dust export from inner Asia is documented by higher glacial stage quartz and mica contents. Dust falls possibly accelerated and intensified the descent of organic matter from sea surface into the abyss by ballasting. The more rapid sinking of POM through the less ventilated deep Pacific Ocean may have lowered biogenic barite formation and raised TOC export, which can possibly account for the observed anticorrelation of TOC (glacial maxima) and Ba/Ti (interglacial maxima), but sedimentary barite dissolution is equally possible.

As the suboxic reduction of detrital magnetite with POM is very slow, we estimate that the observed pervasive magnetite alteration required far more contact time with OM than the short exposure to suboxic bottom water before burial could have provided. Only the long-term coexistence of buried iron oxides and reactive carbon could have enabled microbial communities to successively use most of the sedimentary iron oxides as electron acceptors for organic carbon degradation. Under these premises, enhanced glacial POM accumulation rates paired with far better OM preservation conditions in the suboxic sediment should have resulted in temporary carbon trapping as a prerequisite for the Fe(III) reduction.

When bottom water circulation reestablished during deglaciation, the oxygenation of the seabed should have caused a rapid burn down of still reactive sedimentary organic carbon, causing an important release of CO₂ into the ocean and further into the atmosphere. We estimate that the temporary glacial storage capacity of the abyssal northwest Pacific could amount to ~10 kg C per m² corresponding to 30 Pg C for the total area. Extrapolating this value to all other Pacific basins below 4500 m yields a potential cumulative deglacial CO₂ release of up to 650 Pg C, far more than the glacial-interglacial atmospheric CO₂ shift of 170 Pg C. Clearly, this number is an upper limit and the estimated oceanic DIC and dissolved organic carbon (DOC) reservoirs are much larger, but the long-term retention and rapid deglacial release capacity of sediment-trapped carbon could still be a nonnegligible positive feedback of Quaternary climate cycles. The reduced oxygenation of the abyssal North Pacific Ocean, which our records suggest, should have also increased the residence time of DOC.

A comparison of our time series to other published records supports the idea that the MPT interim phase ended with a modified glacial LCDW/AABW partitioning from the abyssal South Atlantic to the more spacious abyssal Indo-Pacific. The North Pacific seems to have encountered more efficient carbon trapping at the same time when 100 kyr ice age cyclicity fully established. Even if this did not cause a lowered glacial atmospheric pCO₂, it may have increased oceanic carbon retention times and supported longer ice ages.

Acknowledgments

The work of L. Korff was funded by the Federal Ministry of Education and Research (BMBF, Germany) project 03G0202A (INOPEX) and special funds of MARUM, Center for Marine Environmental Sciences, Bremen. We thank the captain, crew, and scientific party of R/V Sonne cruise SO202 for their excellent support during sample collection. We also owe many thanks to L. Brück, C. Hilgenfeldt, H. Piero, and M. Castex (UB), as well as to O. Kreft, L. Baumann, J. Hansen, S. Wiebe and R. Fröhlking (AWI), for laboratory assistance. T. Yamazaki, S. Jaccard, F. Bassinot, and I. Hall kindly provided published data for comparison and correlation. Comments by B. Maher, B. Hönisch, and an unknown reviewer greatly helped to improve this publication and were highly appreciated. All new data of this study are made available at Pangaea data base (www.pangaea.de).

References

- Adkins, J. F. (2013), The role of deep ocean circulation in setting glacial climates, *Paleoceanography*, 28, 539–561, doi:10.1002/palo.20046.
- Alekseeva, V. A., and M. W. Hounslow (2004), Classic sediment source characterisation using discrete and included magnetic particles—Their relationship to conventional petrographic methods in early Pleistocene fluvial-glacial sediments, Upper Don River Basin (Russia), *Phys. Chem. Earth.*, 29, 961–971, doi:10.1016/j.pce.2004.06.003.
- Aoki, K. (2008), Revised age and distribution of ca. 87 ka Aso-4 tephra based on new evidence from the northwest Pacific Ocean, *Quat. Int.*, 178(1), 100–118, doi:10.1016/j.quaint.2007.02.005.
- Balsam, W., B. Ellwood, and J. Ji (2005), Direct correlation of the marine oxygen isotope record with the Chinese Loess Plateau iron oxide and magnetic susceptibility records, *Palaeogeogr. Palaeoclimatol. Palaeoecol.*, 221, 141–152, doi:10.1016/j.palaeo.2005.02.009.
- Bassinot, F. C., L. Beaufort, E. Vincent, L. D. Labeyrie, F. Rostek, P. J. Müller, X. Quidelleur, and Y. Lancelot (1994), Coarse fraction fluctuations in pelagic carbonate sediments from the tropical Indian Ocean: A 1500-kyr record of carbonate dissolution, *Paleoceanography*, 9(4), 579–600, doi:10.1029/94PA00860.
- Bazylinski, D. A., R. B. Frankel, A. J. Garratt-Reed, and S. Mann (1991), Biomineralization of iron sulfides in magnetotactic bacteria from sulfidic environments, *Iron Biominer.*, 239–255, doi:10.1007/978-1-4615-3810-3.
- Berger, W. H., C. G. Adelseck Jr., and L. A. Mayer (1976), Distribution of carbonate in surface sediments of the Pacific Ocean, *J. Geophys. Res.*, 81(15), 2617–2627, doi:10.1029/JC081i015p02617.
- Bishop, J. K. B. (1988), The barite-opal-organic carbon association in oceanic particulate matter, *Nature*, 332(6162), 341–343, doi:10.1038/332341a0.
- Blank, M., M. Leinen, and J. Prospero (1985), Major Asian aeolian inputs indicated by the mineralogy of aerosols and sediments in the western North Pacific, *Nature*, 314(6006), 84–86, doi:10.1038/314084a0.
- Bleil, U. (1985), The magnetostratigraphy of Northwest Pacific sediments, Deep Sea Drilling Project Leg 86, in *Init. Repts. DSDP*, vol. 86, edited by G. R. Heath et al., pp. 441–458, U.S. Gov. Print. Off., Washington, D. C., doi:10.2973/dsdp.proc.86.117.1985.
- Bloemendal, J., J. W. King, F. R. Hall, and S.-J. Doh (1992), Rock magnetism of Late Neogene and Pleistocene deep-sea sediments: Relationship to sediment source, diagenetic processes, and sediment lithology, *J. Geophys. Res.*, 97(B4), 4361–4375, doi:10.1029/91JB03068.
- Bradt Miller, L. I., R. F. Anderson, J. P. Sachs, and M. Q. Fleisher (2010), A deeper respired carbon pool in the glacial equatorial Pacific Ocean, *Earth Planet. Sci. Lett.*, 299(3–4), 417–425, doi:10.1016/j.epsl.2010.09.022.
- Bralower, T. J., and H. R. Thierstein (1984), Low productivity and slow deep-water circulation in mid-Cretaceous oceans, *Geology*, 12(10), 614–618, doi:10.1130/0091-7613(1984)12<614:LPASDC>2.0.CO;2.
- Broecker, W., S. Barker, E. Clark, I. Hajdas, G. Bonani, and L. Stott (2004), Ventilation of the glacial deep Pacific Ocean, *Science*, 306, 1169–1172, doi:10.1126/science.1102293.
- Chang, S. R., and J. L. Kirschvink (1989), Magnetofossils, the magnetization of sediments, and the evolution of magnetite biomineralization, *Annu. Rev. Earth Planet. Sci.*, 17, 169–195, doi:10.1146/annurev.ea.17.050189.001125.
- Dehairs, F., R. Chesselet, and J. Jedwab (1980), Discrete suspended particles of barite and the barium cycle in the open ocean, *Earth Planet. Sci. Lett.*, 49(2), 528–550, doi:10.1016/0012-821X(80)90094-1.
- Dickens, G. R., M. Kölling, D. C. Smith, and L. Schnieders (2007), Rhizon sampling of pore waters on scientific drilling expeditions: An example from the IODP expedition 302, Arctic Coring Expedition (ACEX), *Sci. Drill.*, 4, 22–25, doi:10.2204/iodp.sd.4.08.2007.
- Diekmann, B., and G. Kuhn (2002), Sedimentary record of the mid-Pleistocene climate transition in the southeastern South Atlantic (ODP Site 1090), *Palaeogeogr. Palaeoclimatol. Palaeoecol.*, 182, 241–258, doi:10.1016/S0031-0182(01)00498-9.

- Dillon, M., and C. Franke (2009), Diagenetic alteration of natural Fe-Ti oxides identified by energy dispersive spectroscopy and low-temperature magnetic remanence and hysteresis measurements, *Phys. Earth Planet. Inter.*, 172(3-4), 141–156, doi:10.1016/j.pepi.2008.08.003.
- Dillon, M., and U. Bleil (2006), Rock magnetic signatures in diagenetically altered sediments from the Niger deep-sea fan, *J. Geophys. Res.*, 111, B03105, doi:10.1029/2004JB003540.
- Doh, S.-J., J. W. King, and M. Leinen (1988), A rock-magnetic study of giant piston core LL44-GPC3 from the central North Pacific and its paleoceanographic implications, *Paleoceanography*, 3(1), 89–111, doi:10.1029/PA003i001p00089.
- Duplessy, J. C., N. J. Shackleton, R. G. Fairbanks, L. Labeyrie, D. Oppo, and N. Kallel (1988), Deepwater source variations during the last climatic cycle and their impact on the global deepwater circulation, *Paleoceanography*, 3(3), 343–360, doi:10.1029/PA003i003p00343.
- Dymond, J., E. Suess, and M. Lyle (1992), Barium in deep-sea sediment: A geochemical proxy for paleoproductivity, *Paleoceanography*, 7(2), 163–181, doi:10.1029/92PA00181.
- Emiroğlu, S., D. Rey, and N. Petersen (2004), Magnetic properties of sediments in the R'á de Arousa (Spain): Dissolution of iron oxides and formation of iron sulphides, *Phys. Chem. Earth*, 29, 947–959, doi:10.1016/j.pce.2004.03.012.
- Frederichs, T., U. Bleil, K. Däumler, T. von Dobeneck, and A. Schmidt (1999), The magnetic view on the marine paleoenvironment: Parameters, techniques and potentials of rock magnetic studies as a key to paleoclimatic and paleoceanographic changes, in *Use of Proxies in Paleocyanography: Examples from the South Atlantic*, edited by G. Fischer and G. Wefer, pp. 575–599, Springer, Berlin, doi:10.1007/978-3-642-58646-0_24.
- Fu, Y., T. von Dobeneck, C. Franke, D. Heslop, and S. Kasten (2008), Rock magnetic identification and geochemical process models of greigite formation in Quaternary marine sediments from the Gulf of Mexico (IODP Hole U1319A), *Earth Planet. Sci. Lett.*, 275(3-4), 233–245, doi:10.1016/j.epsl.2008.07.034.
- Fukasawa, M., H. Freeland, R. Perkin, T. Watanabe, H. Uchida, and A. Nishina (2004), Bottom water warming in the North Pacific Ocean, *Nature*, 427(6977), 825–827, doi:10.1038/nature02337.
- Funk, J. A., T. von Dobeneck, and A. Reitz (2004a), Integrated rock magnetic and geochemical quantification of redoxomorphic iron mineral diagenesis in Late Quaternary sediments from the Equatorial Atlantic, in *The South Atlantic in the Late Quaternary: Reconstruction of Material Budgets and Current Systems*, edited by G. Wefer, S. Mulitza, and V. Ratmeyer, pp. 237–260, Springer, Berlin, doi:10.1007/978-3-642-18917-3_12.
- Funk, J. A., T. von Dobeneck, T. Wagner, and S. Kasten (2004b), Late Quaternary sedimentation and early diagenesis in the equatorial Atlantic Ocean: Patterns, trends and processes deduced from rock magnetic and geochemical records, in *The South Atlantic in the Late Quaternary: Reconstruction of Material Budgets and Current Systems*, edited by G. Wefer, S. Mulitza, and V. Ratmeyer, pp. 461–497, Springer, Berlin, doi:10.1007/978-3-642-18917-3_21.
- Galbraith, E. D., S. L. Jaccard, T. F. Pedersen, D. M. Sigman, G. H. Haug, M. Cook, J. R. Southon, and R. Francois (2007), Carbon dioxide release from the North Pacific abyss during the last deglaciation, *Nature*, 449(7164), 890–893, doi:10.1038/nature06227.
- Galbraith, E. D., M. Kienast, S. L. Jaccard, T. F. Pedersen, B. G. Brunelle, D. M. Sigman, and T. Kiefer (2008), Consistent relationship between global climate and surface nitrate utilization in the western subarctic Pacific throughout the last 500 ka, *Paleoceanography*, 23, PA2212, doi:10.1029/2007PA001518.
- Ganeshram, R. S., R. Francois, J. Commeau, and S. L. Brown-Leger (2003), An experimental investigation of barite formation in seawater, *Geochim. Cosmochim. Acta*, 67(14), 2599–2605, doi:10.1016/S0016-7037(03)00164-9.
- Garming, J. F. L., U. Bleil, and N. Riedinger (2005), Alteration of magnetic mineralogy at the sulphate-methane transition: Analysis of sediments from the Argentine continental slope, *Phys. Earth Planet. Inter.*, 151, 290–308, doi:10.1016/j.pepi.2005.04.001.
- Gebhardt, H., M. Sarnthein, P. M. Grootes, T. Kiefer, H. Kuehn, F. Schmieder, and U. Röhl (2008), Paleonutrient and productivity records from the subarctic North Pacific for Pleistocene glacial terminations I to V, *Paleoceanography*, 23, PA4212, doi:10.1029/2007PA001513.
- Gersonde, R. (2012), The expedition of the research vessel “Sonne” to the subpolar North Pacific and the Bering Sea in 2009 (SO202-INOPEX) Reports on polar and marine research, Bremerhaven, Alfred Wegener Institute for Polar and Marine Research, 643, 323 pp., hdl:10013/epic.38996.
- Gingele, F., and A. Dahmke (1994), Discrete barite particles and barium as tracers of paleoproductivity in South Atlantic sediments, *Paleoceanography*, 9(1), 151–168, doi:10.1029/93PA02559.
- Gingele, F. X., M. Zabel, S. Kasten, W. J. Bonn, and C. C. Nürnberg (1999), Biogenic barium as a proxy for paleoproductivity: Methods and limitations of application, in *Use of Proxies in Paleocyanography: Examples from the South Atlantic*, edited by G. Fischer and G. Wefer, pp. 345–364, Springer, Berlin, doi:10.1007/978-3-642-58646-0_13.
- Hain, M. P., D. M. Sigman, and G. H. Haug (2011), Shortcomings of the isolated abyssal reservoir model for deglacial radiocarbon changes in the mid-depth Indo-Pacific Ocean, *Geophys. Res. Lett.*, 38, L04604, doi:10.1029/2010GL046158.
- Hall, I. R., I. N. McCave, N. J. Shackleton, G. P. Weedon, and S. E. Harris (2001), Intensified deep Pacific inflow and ventilation in Pleistocene glacial times, *Nature*, 412, 809–812, doi:10.1038/35090552.
- Hansell, D. A., and C. A. Carlson (2013), Localized refractory dissolved organic carbon sinks in the deep ocean, *Global Biogeochem. Cycles*, 27, 705–710, doi:10.1002/gbc.20067.
- Hartnett, H. E., R. G. Keil, J. I. Hedges, and A. H. Devol (1998), Influence of oxygen exposure time on organic carbon preservation in continental margin sediments, *Nature*, 391(6667), 572–574, doi:10.1038/35351.
- Hepp, D. A., T. Mörz, C. Hensen, T. Frederichs, S. Kasten, N. Riedinger, and W. W. Hay (2009), A late Miocene-early Pliocene Antarctic deepwater record of repeated iron reduction events, *Mar. Geol.*, 266(1-4), 198–211, doi:10.1016/j.margeo.2009.08.006.
- Herguera, J. C., E. Jansen, and W. H. Berger (1992), Evidence for a bathyal front at 2000 m depth in the glacial Pacific, based on a depth transect on Ontong Java Plateau, *Paleoceanography*, 7(3), 273–288, doi:10.1029/92PA00869.
- Herguera, J. C., T. Herbert, M. Kashgarian, and C. Charles (2010), Intermediate and deep water mass distribution in the Pacific during the Last Glacial Maximum inferred from oxygen and carbon stable isotopes, *Quat. Sci. Rev.*, 29(9-10), 1228–1245, doi:10.1016/j.quascirev.2010.02.009.
- Hong, C.-S., M.-Y. Lee, H. Pälike, K.-Y. Wei, W.-T. Liang, Y. Izuka, and M. Torii (2002), Astronomically calibrated ages for geomagnetic reversals within the Matuyama chron, *Earth Planets Space*, 54(6), 679–690, doi:10.1186/BF03351719.
- Hounslow, M. W., and B. A. Maher (1999), Source of the climate signal recorded by magnetic susceptibility variations in Indian Ocean sediments, *J. Geophys. Res.*, 104(B3), 5047–5061, doi:10.1029/1998JB900085.
- Hovan, S. A., D. K. Rea, N. G. Pisias, and N. J. Shackleton (1989), A direct link between the China loess and marine $\delta^{18}\text{O}$ records: Aeolian flux to the North Pacific, *Nature*, 340(6231), 296–298, doi:10.1038/340296a0.
- Hovan, S. A., D. K. Rea, and N. G. Pisias (1991), Late Pleistocene continental climate and oceanic variability recorded in northwest Pacific sediments, *Paleoceanography*, 6(3), 349–370, doi:10.1029/91PA00559.
- Itambi, A. C., T. von Dobeneck, S. Mulitza, T. Bickert, and D. Heslop (2009), Millennial-scale northwest African droughts related to Heinrich events and Dansgaard-Oeschger cycles: Evidence in marine sediments from offshore Senegal, *Paleoceanography*, 24, PA1205, doi:10.1029/2007PA001570.

- Jaccard, S. L., G. H. Haug, D. M. Sigman, T. F. Pedersen, H. R. Thierstein, and U. Röhl (2005), Glacial/interglacial changes in subarctic North Pacific stratification, *Science*, *308*(5724), 1003–1006, doi:10.1126/science.1108696.
- Jaccard, S. L., E. D. Galbraith, D. M. Sigman, G. H. Haug, R. Francois, T. F. Pedersen, P. Dulski, and H. R. Thierstein (2009), Subarctic Pacific evidence for a glacial deepening of the oceanic respired carbon pool, *Earth Planet. Sci. Lett.*, *277*(1–2), 156–165, doi:10.1016/j.epsl.2008.10.017.
- Jaccard, S. L., E. D. Galbraith, D. M. Sigman, and G. H. Haug (2010), A pervasive link between Antarctic ice core and subarctic Pacific sediment records over the past 800 kyrs, *Quat. Sci. Rev.*, *29*(1–2), 206–212, doi:10.1016/j.quascirev.2009.10.007.
- Jaccard, S. L., E. D. Galbraith, A. Martínez-García, and R. F. Anderson (2016), Covariation of deep Southern Ocean oxygenation and atmospheric CO₂ through the last ice age, *Nature*, doi:10.1038/nature16514.
- Jaccard, S. L., and E. D. Galbraith (2013), Direct ventilation of the North Pacific did not reach the deep ocean during the last deglaciation, *Geophys. Res. Lett.*, *40*, 199–203, doi:10.1029/2012GL054118.
- Just, J., M. J. Dekkers, T. von Dobeneck, A. van Hoesel, and T. Bickert (2012), Signatures and significance of aeolian, fluvial, bacterial and diagenetic magnetic mineral fractions in Late Quaternary marine sediments off Gambia, NW Africa, *Geochem. Geophys. Geosyst.*, *13*, Q0A002, doi:10.1029/2012GC004146.
- Karlin, R. (1990), Magnetic Mineral diagenesis in suboxic sediments at Bettis site W-N, NE Pacific Ocean, *J. Geophys. Res.*, *95*(B4), 4421–4436, doi:10.1029/JB095iB04p04421.
- Karlin, R., M. Lyle, and G. R. Heath (1987), Authigenic magnetite formation in suboxic marine sediments, *Nature*, *326*, 490–493, doi:10.1038/326490a0.
- Kasten, S., R. R. Haese, M. Zabel, C. Rühlemann, and H. D. Schulz (2001), Barium peaks at glacial terminations in sediments of the equatorial Atlantic Ocean—Relicts of deglacial productivity pulses?, *Chem. Geol.*, *175*(3–4), 635–651, doi:10.1016/S0009-2541(00)00377-6.
- Kawabe, M., S. Fujio, D. Yanagimoto, and T. Tanaka (2009), Water masses and currents of deep circulation southwest of the Shatsky Rise in the western North Pacific, *Deep Sea Res., Part I*, *56*(10), 1675–1687, doi:10.1016/j.dsr.2009.06.003.
- Keigwin, L. D. (1998), Glacial-age hydrography of the far northwest Pacific Ocean, *Paleoceanography*, *13*(4), 323–339, doi:10.1029/98PA00874.
- Kent, D. V., and W. Lowrie (1974), Origin of magnetic instability in sediment cores from the central North Pacific, *J. Geophys. Res.*, *79*(20), 2987–3000, doi:10.1029/JB079i020p02987.
- King, J., S. K. Banerjee, J. Marvin, and Ö. Özdemir (1982), A comparison of different magnetic methods for determining the relative grain size of magnetite in natural materials: Some results from lake sediments, *Earth Planet. Sci. Lett.*, *59*(2), 404–419, doi:10.1016/0012-821X(82)90142-X.
- Kirschvink, J. L. (1980), The least-squares line and plane and the analysis of paleomagnetic data, *Geophys. J. R. Astron. Soc.*, *62*(3), 699–718, doi:10.1111/j.1365-246X.1980.tb02601.x.
- Knudson, K. P., and A. C. Ravelo (2015), North Pacific Intermediate Water circulation enhanced by the closure of the Bering Strait, *Paleoceanography*, *30*, 1287–1304, doi:10.1002/2015PA002840.
- Kohfeld, K. E., and S. P. Harrison (2001), DIRTMAP: The geological record of dust, *Earth Sci. Rev.*, *54*(1–3), 81–114, doi:10.1016/S0012-8252(01)00042-3.
- Larrasoaña, J. C., A. P. Roberts, J. S. Stoner, C. Richter, and R. Wehausen (2003), A new proxy for bottom-water ventilation in the eastern Mediterranean based on diagenetically controlled magnetic properties of sapropel-bearing sediments, *Palaeogeogr. Palaeoclimatol. Palaeoecol.*, *190*, 221–242, doi:10.1016/S0031-0182(02)00607-7.
- Lechtenfeld, O. J., G. Kattner, R. Flerus, S. L. McCallister, P. Schmitt-Kopplin, and B. P. Koch (2014), Molecular transformation and degradation of refractory dissolved organic matter in the Atlantic and Southern Ocean, *Geochim. Cosmochim. Acta*, *126*(1), 321–337, doi:10.1016/j.gca.2013.11.009.
- Leslie, B. W., S. P. Lund, and D. E. Hammond (1990), Rock magnetic evidence for the dissolution and authigenic growth of magnetic minerals within anoxic marine sediments of the California continental borderland, *J. Geophys. Res.*, *95*, 4437–4452, doi:10.1029/JB095iB04p04437.
- Lisiecki, L. E., and M. E. Raymo (2005), A Pliocene-Pleistocene stack of 57 globally distributed benthic $\delta^{18}\text{O}$ records, *Paleoceanography*, *20*, PA1003, doi:10.1029/2004PA001071.
- Liu, J., R. Zhu, A. P. Roberts, S. Li, and J.-H. Chang (2004), High-resolution analysis of early diagenetic effects on magnetic minerals in post-middle-Holocene continental shelf sediments from the Korean Strait, *J. Geophys. Res.*, *109*, B03103, doi:10.1029/2003JB002813.
- Maasch, K. A. (1988), Statistical detection of the Mid-Pleistocene transition, *Clim. Dyn.*, *2*(3), 133–143, doi:10.1007/BF01053471.
- Maeda, L., H. Kawahata, and M. Nohara (2002), Fluctuation of biogenic and abiogenic sedimentation on the Shatsky Rise in the western North Pacific during the late Quaternary, *Mar. Geol.*, *189*(3–4), 197–214, doi:10.1016/S0025-3227(02)00405-X.
- Maher, B. A. (1988), Magnetic properties of some synthetic sub-micron magnetites, *Geophys. J. R. Astron. Soc.*, *94*(1), 83–96, doi:10.1111/j.1365-246X.1988.tb03429.x.
- Maher, B. A., and R. Thompson (1999), *Quaternary Climates, Environments and Magnetism*, 412 pp., Cambridge Univ. Press, Cambridge, U. K.
- Maher, B. A., J. M. Prospero, D. Mackie, D. Gaiero, P. P. Hesse, and Y. Balkanski (2010), Global connections between aeolian dust, climate and ocean biogeochemistry at the present day and at the last glacial maximum, *Earth Sci. Rev.*, *99*(1–2), 61–97, doi:10.1016/j.earscirev.2009.12.001.
- Martin, J. H., G. A. Knauer, D. M. Karl, and W. W. Broenkow (1987), VERTEX: Carbon cycling in the northeast Pacific, *Deep Sea Res., Part A*, *34*, 267–285, doi:10.1016/0198-0149(87)90086-0.
- Maslin, M. A., X. S. Li, M.-F. Loutre, and A. Berger (1998), The contribution of orbital forcing to the progressive intensification of Northern Hemisphere glaciations, *Quat. Sci. Rev.*, *17*(4–5), 411–426, doi:10.1016/S0277-3791(97)00047-4.
- Matsumoto, K. (2007), Biology-mediated temperature control on atmospheric pCO₂ and ocean biogeochemistry, *Geophys. Res. Lett.*, *34*, L20605, doi:10.1029/2007GL031301.
- Matsumoto, K., T. Oba, J. Lynch-Stieglitz, and H. Yamamoto (2002), Interior hydrography and circulation of the glacial Pacific Ocean, *Quat. Sci. Rev.*, *21*(14–15), 1693–1704, doi:10.1016/S0277-3791(01)00142-1.
- Mills, R. A., S. L. Taylor, H. Pälike, and J. Thomson (2010), Hydrothermal sediments record changes in deep water oxygen content in the SE Pacific, *Paleoceanography*, *25*, PA4226, doi:10.1029/2010PA001959.
- Mudelsee, M., and M. Schulz (1997), The Mid-Pleistocene climate transition: Onset of 100 ka cycle lags ice volume build-up by 280 ka, *Earth Planet. Sci. Lett.*, *151*(1–2), 117–123, doi:10.1016/S0012-821X(97)00114-3.
- Müller, P. J., and R. Schneider (1993), An automated leaching method for the determination of opal in sediments and particulate matter, *Deep Sea Res., Part I*, *40*(3), 425–444, doi:10.1016/0967-0637(93)90140-X.
- Nakanishi, M., K. Tamaki, and K. Kobayashi (1989), Mesozoic magnetic anomaly lineations and seafloor spreading history of the northwestern Pacific, *J. Geophys. Res.*, *94*(B11), 15,437–15,462, doi:10.1029/JB094iB11p15437.
- Natland, J. H. (1993), Volcanic ash and pumice at Shatsky Rise: Sources, mechanisms of transport, and bearing on atmospheric circulation, in *Proc. ODP, Sci. Results*, vol. 132, edited by J.H. Natland et al., 57–66, Ocean Drilling Program, College Station, Tex., doi:10.2973/odp.proc.sr.132.301.1993.

- Nichol, J. E., and D. W. Nichol (2013), Pleistocene loess in the humid subtropical forest zone of East Asia, *Geophys. Res. Lett.*, *40*, 1978–1983, doi:10.1002/grl.50426.
- Nilson, E., and F. Lehmkuhl (2001), Interpreting temporal patterns in the late Quaternary dust flux from Asia to the North Pacific, *Quat. Int.*, *76/77*, 67–76, doi:10.1016/S1040-6182(00)00090-2.
- Ninkovich, D., N. Opdyke, B. C. Heezen, and J. H. Foster (1966), Paleomagnetic stratigraphy, rates of deposition and tephrochronology in North Pacific deep-sea sediments, *Earth Planet. Sci. Lett.*, *1*(6), 476–492, doi:10.1016/0012-821X(66)90052-5.
- Ohkushi, K., A. Suzuki, H. Kawahata, and L. P. Gupta (2003), Glacial-interglacial deep-water changes in the NW Pacific inferred from single foraminiferal $\delta^{18}\text{O}$ and $\delta^{13}\text{C}$, *Mar. Micropaleontol.*, *48*(3–4), 281–290, doi:10.1016/S0377-8398(03)00023-9.
- Okazaki, Y., A. Timmermann, L. Menviel, N. Harada, A. Abe-Ouchi, M. O. Chikamoto, A. Mouchet, and H. Asahi (2010), Deepwater formation in the North Pacific during the last glacial termination, *Science*, *329*(5988), 200–204, doi:10.1126/science.1190612.
- Okazaki, Y., T. Sagawa, H. Asahi, K. Horikawa, and J. Onodera (2012), Ventilation changes in the western North Pacific since the last glacial period, *Clim. Past*, *8*(1), 17–24, doi:10.5194/cp-8-17-2012.
- Owens, W. B., and B. A. Warren (2001), Deep circulation in the northwest corner of the Pacific Ocean, *Deep Sea Res., Part I*, *48*(4), 959–993, doi:10.1016/S0967-0637(00)00076-5.
- Pälike, H., R. D. Norris, J. O. Herrle, P. A. Wilson, H. K. Coxall, C. H. Lear, N. J. Shackleton, A. K. Tripathi, and B. S. Wade (2006), The heartbeat of the Oligocene climate system, *Science*, *314*(5807), 1894–1898, doi:10.1126/science.1133822.
- Paytan, A., and M. Kastner (1996), Benthic Ba fluxes in the central Equatorial Pacific, implications for the oceanic Ba cycle, *Earth Planet. Sci. Lett.*, *142*(3–4), 439–450, doi:10.1016/0012-821X(96)00120-3.
- Pfeifer, K., S. Kasten, C. Hensen, and H. D. Schulz (2001), Reconstruction of primary productivity from the barium contents in surface sediments of the South Atlantic Ocean, *Mar. Geol.*, *177*(1–2), 13–24, doi:10.1016/S0025-3227(01)00121-9.
- Raymo, M. E., D. W. Oppo, and W. Curry (1997), The Mid-Pleistocene climate transition: A deep sea carbon isotope perspective, *Paleoceanography*, *12*(4), 546–559, doi:10.1029/97PA01019.
- Rea, D. K. (1994), The paleoclimatic record provided by eolian deposition in the deep sea: The geologic history of wind, *Rev. Geophys.*, *32*(2), 159–195, doi:10.1029/93RG03257.
- Reid, J. L., and P. F. Lonsdale (1974), On the flow of water through the Samoan Passage, *J. Phys. Oceanogr.*, *4*, 58–73, doi:10.1175/1520-0485(1974)004<0058:OTFOWT>2.0.CO;2.
- Reitz, A., K. Pfeifer, G. J. de Lange, and J. Klump (2004), Biogenic barium and the detrital Ba/Al ratio: A comparison of their direct and indirect determination, *Mar. Geol.*, *204*(3–4), 289–300, doi:10.1016/S0025-3227(04)00004-0.
- Riedinger, N., S. Kasten, J. Gröger, C. Franke, and K. Pfeifer (2006), Active and buried authigenic barite fronts in sediments from the Eastern Cape Basin, *Earth Planet. Sci. Lett.*, *241*(3–4), 876–888, doi:10.1016/j.epsl.2005.10.032.
- Roberts, A. P. (2008), Geomagnetic excursions: Knowns and unknowns, *Geophys. Res. Lett.*, *35*, L17307, doi:10.1029/2008GL034719.
- Roberts, A. P., B. Lehman, R. J. Weeks, K. L. Verosub, and C. Laj (1997), Relative paleointensity of the geomagnetic field over the last 200,000 years from ODP Sites 883 and 884, North Pacific Ocean, *Earth Planet. Sci. Lett.*, *152*(1–4), 11–23, doi:10.1016/S0012-821X(97)00132-5.
- Roberts, A. P., J. S. Stoner, and C. Richter (1999), Diagenetic magnetic enhancement of sapropels from the eastern Mediterranean Sea, *Mar. Geol.*, *153*(1–4), 103–116, doi:10.1016/S0025-3227(98)00087-5.
- Robinson, S. G., J. T. S. Sahota, and F. Oldfield (2000), Early diagenesis in North Atlantic abyssal plain sediments characterized by rock-magnetic and geochemical indices, *Mar. Geol.*, *163*, 77–107, doi:10.1016/S0025-3227(99)00108-5.
- Ronge, T. A., S. Steph, R. Tiedemann, M. Prange, U. Merkel, D. Nürnberg, and G. Kuhn (2015), Pushing the boundaries: Glacial/interglacial variability of intermediate and deep waters in the southwest Pacific over the last 350,000 years, *Paleoceanography*, *30*, 23–38, doi:10.1002/2014PA002727.
- Schmidt, A., T. von Dobeneck, and U. Bleil (1999), Magnetic characterization of Holocene sedimentation in the South Atlantic, *Paleoceanography*, *14*(4), 465–481, doi:10.1029/1999PA900020.
- Schmieder, F., T. von Dobeneck, and U. Bleil (2000), The Mid-Pleistocene climate transition as documented in the deep South Atlantic Ocean: Initiation, interim state and terminal event, *Earth Planet. Sci. Lett.*, *179*(3–4), 539–549, doi:10.1016/S0012-821X(00)00143-6.
- Seeberg-Elverfeldt, J., M. Schlüter, T. Feseker, and M. Kölling (2005), Rhizon sampling of porewaters near the sediment-water interface of aquatic systems, *Limnol. Oceanogr. Methods*, *3*, 361–371, doi:10.4319/lom.2005.3.361.
- Serno, S., G. Winckler, R. F. Anderson, C. T. Hayes, H. Ren, R. Gersonde, and G. H. Haug (2014), Using the natural spatial pattern of marine productivity in the Subarctic North Pacific to evaluate paleoproductivity proxies, *Paleoceanography*, *29*, 438–453, doi:10.1002/2013PA002594.
- Sexton, P. F., and S. Barker (2012), Onset of 'Pacific-style' deep-sea sedimentary carbonate cycles at the mid-Pleistocene transition, *Earth Planet. Sci. Lett.*, *321*–322, 81–94, doi:10.1016/j.epsl.2011.12.043.
- Shigemitsu, M., H. Narita, Y. W. Watanabe, N. Harada, and S. Tsunogai (2007), Ba, Si, U, Al, Sc, La, Th, C and $^{13}\text{C}/^{12}\text{C}$ in a sediment core in the western subarctic Pacific as proxies of past biological production, *Mar. Chem.*, *106*(3–4), 442–455, doi:10.1016/j.marchem.2007.04.004.
- Sigman, D. M., and E. A. Boyle (2000), Glacial/interglacial variations in atmospheric carbon dioxide, *Nature*, *407*(6806), 859–869, doi:10.1038/35038000.
- Sigman, D. M., M. P. Hain, and G. H. Haug (2010), The polar ocean and glacial cycles in atmospheric CO_2 concentration, *Nature*, *466*(7302), 47–55, doi:10.1038/nature09149.
- St. John, K. E. K., and L. A. Krissek (1999), Regional patterns of Pleistocene ice-rafted debris flux in the North Pacific, *Paleoceanography*, *14*(5), 653–662, doi:10.1029/1999PA900030.
- Stoner, J. S., J. E. T. Channell, and C. Hillaire-Marcel (1996), The magnetic signature of rapidly deposited detrital layers from the deep Labrador Sea: Relationship to North Atlantic Heinrich layers, *Paleoceanography*, *11*(3), 309–325, doi:10.1029/96PA00583.
- Tarduno, J. A. (1994), Temporal trends of magnetic dissolution in the pelagic realm: Gauging paleoproductivity?, *Earth Planet. Sci. Lett.*, *123*(1–3), 39–48, doi:10.1016/0012-821X(94)90255-0.
- Tarduno, J. A., and S. L. Wilkison (1996), Non-steady state magnetic mineral reduction, chemical lock-in, and delayed remanence acquisition in pelagic sediments, *Earth Planet. Sci. Lett.*, *144*(3–4), 315–326, doi:10.1016/S0012-821X(96)00174-4.
- Tauxe, L. (1993), Sedimentary records of relative paleointensity of the geomagnetic field in sediments: Theory and practice, *Rev. Geophys.*, *31*(3), 319–354, doi:10.1029/93RG01771.
- Tauxe, L., T. Herbert, N. J. Shackleton, and Y. S. Kok (1996), Astronomical calibration of the Matuyama-Brunhes boundary: Consequences for magnetic remanence acquisition in marine carbonates and the Asian loess sequences, *Earth Planet. Sci. Lett.*, *140*(1–4), 133–146, doi:10.1016/0012-821X(96)00030-1.
- Thompson, R., and F. Oldfield (1986), *Environmental Magnetism*, 227 pp., Allen and Unwin, London, doi:10.1007/978-94-011-8036-8.
- Thomson, J., T. R. S. Wilson, F. Culklin, and D. J. Hydes (1984), Non-steady state diagenetic record in eastern equatorial Atlantic sediments, *Earth Planet. Sci. Lett.*, *71*(1), 23–30, doi:10.1016/0012-821X(84)90049-9.

- Tjallingii, R., U. Röhl, M. Kölling, and T. Bickert (2007), Influence of the water content on X-ray fluorescence core-scanning measurements in soft marine sediments, *Geochem. Geophys. Geosyst.*, *8*, Q02004, doi:10.1029/2006GC001393.
- Toggweiler, J. R. (1999), Variation of atmospheric CO₂ by ventilation of the ocean's deepest water, *Paleoceanography*, *14*(5), 571–588, doi:10.1029/1999PA900033.
- Tomczak, M., and J. S. Godfrey (2003), *Regional Oceanography: An Introduction*, 2nd ed., p. 390, Daya House, Delhi.
- Torres, M. E., H. J. Brumsack, G. Bohrmann, and K. C. Emeis (1996), Barite fronts in continental margin sediments: A new look at barium remobilization in the zone of sulfate reduction and formation of heavy barites in diagenetic fronts, *Chem. Geol.*, *127*(1-3), 125–139, doi:10.1016/0009-2541(95)00090-9.
- Uchida, H., H. Yamamoto, K. Ichikawa, I. Kaneko, M. Fukasawa, T. Kawano, and Y. Kumamoto (2007), Flow of abyssal water into Wake Island Passage: Properties and transports from hydrographic surveys, *J. Geophys. Res.*, *112*, C04008, doi:10.1029/2006JC004000.
- Valet, J.-P., L. Meynadier, and Y. Guyodo (2005), Geomagnetic dipole strength and reversal rate over the past two million years, *Nature*, *435*(7043), 802–805, doi:10.1038/nature03674.
- Vali, H., T. von Dobeneck, G. Amarantidis, O. Förster, G. Morteani, L. Bachmann, and N. Petersen (1989), Biogenic and lithogenic magnetic minerals in Atlantic and Pacific deep sea sediments and their paleomagnetic significance, *Geol. Rundsch.*, *78*, 753–764, doi:10.1007/BF01829320.
- Venuti, A., F. Florindo, E. Michel, and I. R. Hall (2007), Magnetic proxy for the deep (Pacific) western boundary current variability across the mid-Pleistocene climate transition, *Earth Planet. Sci. Lett.*, *259*, 107–118, doi:10.1016/j.epsl.2007.04.032.
- von Breyann, M. T. K., K. C. Emeis, and E. Suess (1992), Water depth and diagenetic constraints on the use of barium as a paleoproductivity indicator, in *Upwelling Systems: Evolution Since the Early Miocene*, *Geol. Soc. Spec. Publ.*, vol. 64, edited by C. P. Summerhayes et al., pp. 273–284.
- Wallace, H. E., J. Thomson, T. R. S. Wilson, P. P. E. Weaver, N. C. Higgs, and D. J. Hydes (1988), Active diagenetic formation of metal-rich layers in N.E. Atlantic sediments, *Geochim. Cosmochim. Acta*, *52*(6), 1557–1569, doi:10.1016/0016-7037(88)90225-6.
- Wang, P., J. Tian, X. Cheng, C. Liu, and J. Xu (2003), Carbon reservoir changes preceded major ice-sheet expansion at mid-Brunhes event, *Geology*, *31*, 239–242, doi:10.1130/0091-7613(2003)031<0239:CRCPMI>2.0.CO;2.
- Wang, P., J. Tian, and X. Cheng (2004), Major Pleistocene stages in a carbon perspective: The South China Sea record and its global comparison, *Paleoceanography*, *19*, PA4005, doi:10.1029/2003PA000991.
- Wang, P., Q. Y. Li, J. Tian, Z. M. Jian, C. L. Liu, L. Li, and W. T. Ma (2014), Long-term cycles in the carbon reservoir of the Quaternary ocean: A perspective from the South China Sea, *Natl. Sci. Rev.*, *1*, 119–143, doi:10.1093/nsr/nwt028.
- Yamamoto, Y., T. Yamazaki, T. Kanamatsu, N. Ioka, and T. Mishima (2007), Relative paleointensity stack during the last 250 kyr in the northwest Pacific, *J. Geophys. Res.*, *112*, B01104, doi:10.1029/2006JB004477.
- Yamane, M. (2003), Late Quaternary variations in water mass in the Shatsky Rise area, northwest Pacific Ocean, *Mar. Micropaleontol.*, *48*(3-4), 205–223, doi:10.1016/S0377-8398(03)00017-3.
- Yamazaki, T. (1999), Relative paleointensity of the geomagnetic field during Brunhes Chron recorded in North Pacific deep-sea sediment cores: Orbital influence?, *Earth Planet. Sci. Lett.*, *169*(1-2), 23–35, doi:10.1016/S0012-821X(99)00064-3.
- Yamazaki, T., and T. Kanamatsu (2007), A relative paleointensity record of the geomagnetic field since 1.6 Ma from the North Pacific, *Earth Planets Space*, *59*(7), 785–794, doi:10.1186/BF03352741.
- Yamazaki, T., and N. Ioka (1997), Environmental rock-magnetism of pelagic clay: Implications for Asian eolian input to the North Pacific since the Pliocene, *Paleoceanography*, *12*(1), 111–124, doi:10.1029/96PA02757.
- Yamazaki, T., and H. Oda (2005), A geomagnetic paleointensity stack between 0.8 and 3.0 Ma from equatorial Pacific sediment cores, *Geochem. Geophys. Geosyst.*, *6*, Q11H20, doi:10.1029/2005GC001001.
- Yamazaki, T., A. L. Abdeldayem, and K. Ikehara (2003), Rock-magnetic changes with reduction diagenesis in Japan Sea sediments and preservation of geomagnetic secular variation in inclination during the last 30,000 years, *Earth Planets Space*, *55*(6), 327–340, doi:10.1186/BF03351766.
- Yanagimoto, D., and M. Kawabe (2007), Deep-circulation flow at mid-latitude in the western North Pacific, *Deep Sea Res., Part I*, *54*(12), 2067–2081, doi:10.1016/j.dsr.2007.09.004.
- Yanagimoto, D., M. Kawabe, and S. Fujio (2010), Direct velocity measurements of deep circulation southwest of the Shatsky Rise in the western North Pacific, *Deep Sea Res., Part I*, *57*(3), 328–337, doi:10.1016/j.dsr.2009.12.004.
- You, Y. (2003), Implications of cabbeling on the formation and transformation mechanism of North Pacific Intermediate Water, *J. Geophys. Res.*, *108*(C5), 3134, doi:10.1029/2001JC001285.
- You, Y., N. Suginoara, M. Fukasawa, I. Yasuda, I. Kaneko, H. Yoritaka, and M. Kawamiya (2000), Roles of the Okhotsk Sea and Gulf of Alaska in forming the North Pacific Intermediate Water, *J. Geophys. Res.*, *105*(C2), 3253–3280, doi:10.1029/1999JC900304.
- Zonneveld, K. A. F., et al. (2010), Selective preservation of organic matter in marine environments; processes and impact on the sedimentary record, *Biogeosciences*, *7*(2), 483–511, doi:10.5194/bg-7-483-2010.